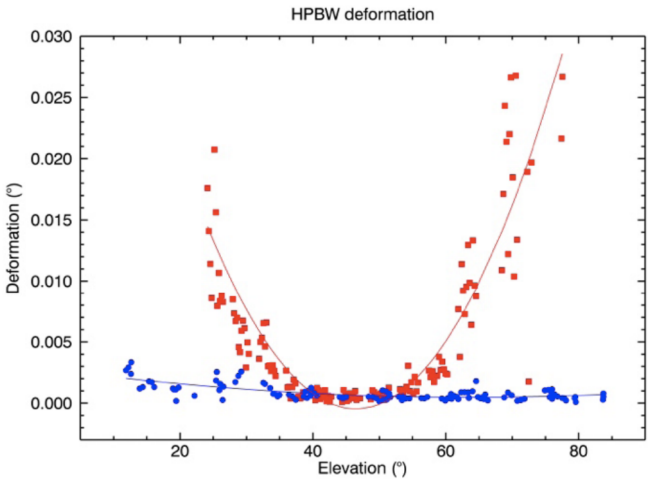

Figure 20: *Beam deformation measured by Bolli et al. (2015) in K-band. Red squares and blue circles indicate data obtained with (i) a fixed optics and (ii) with the active surface plus subreflector in tracking mode, respectively.*

We present the maps of 3C84 obtained with the 7 feeds of the K-band receiver at 60° of elevation in Fig. 21, then the maps of both polarizations (LCP and RCP, which correspond to Ch0 and Ch1 respectively) for each feed (Fig. 22). The noise excess in the maps of the feeds 2 and 4 are due to a well-known instability in the feed 2 and 4 cryogenic LNAs, which will be soon replaced with new ones. LCP of the 5th feed is not usable.

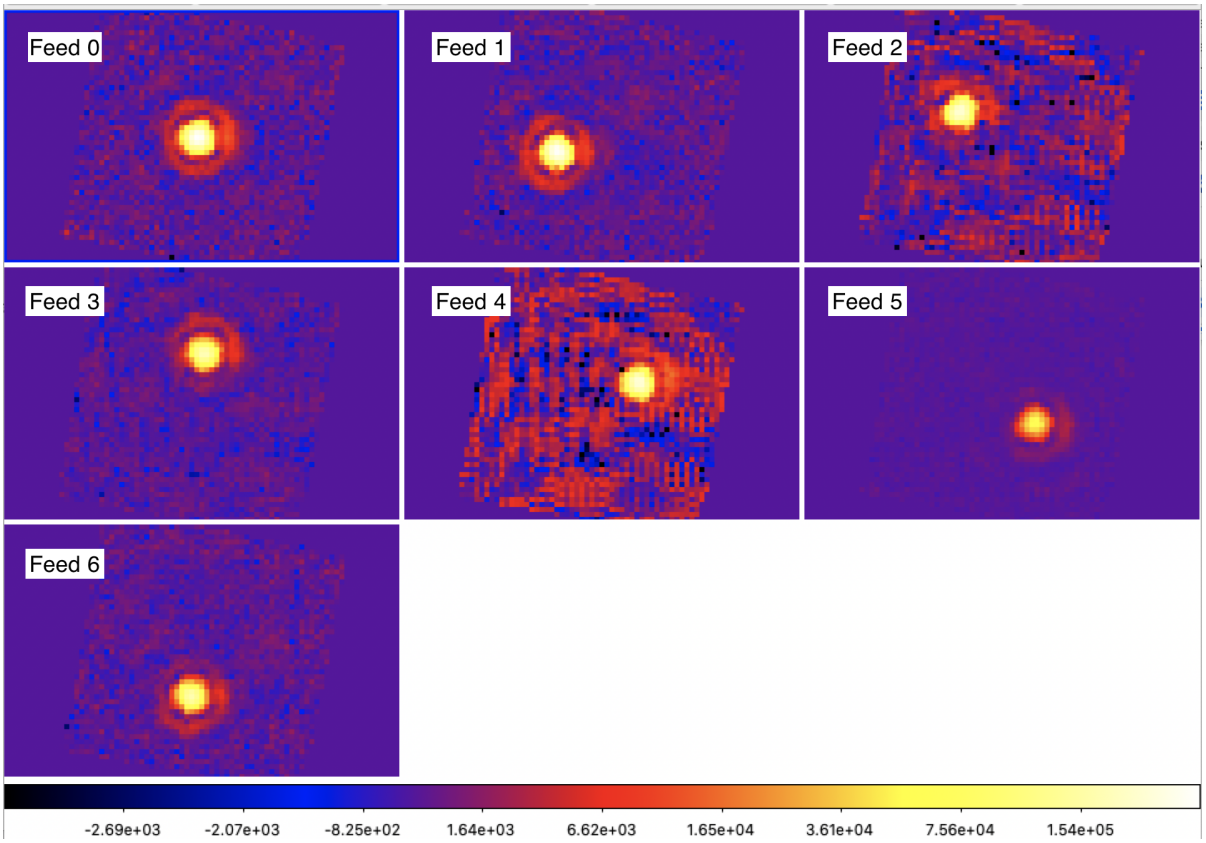

Figure 21: *Maps of 3C84 (0.2°x0.2°) obtained with the 7 feeds at 60°el on 17/12/2020.*

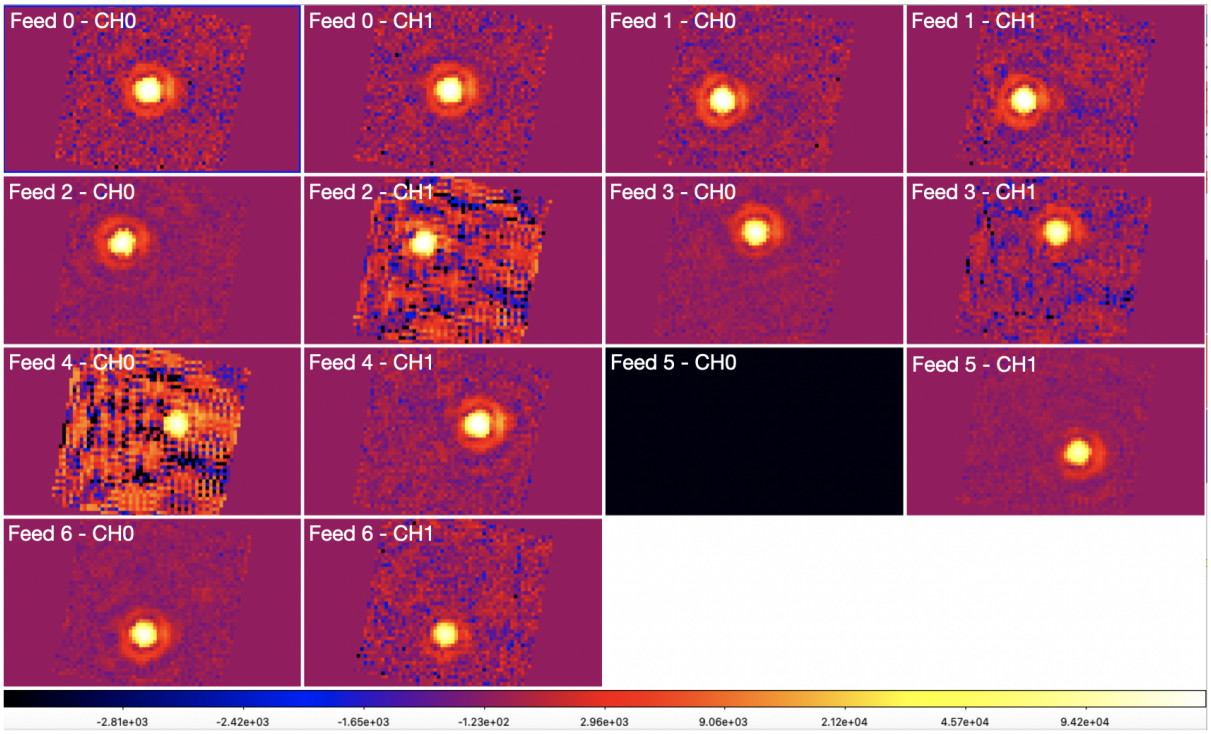

Figure 22: *Maps of 3C84 (0.2°x0.2°) obtained for Ch0 and Ch1 corresponding to the 7 feeds at 60°el on 17/12/2020.*

We report in Table 7 the measurements of the S/N of Ch0 and Ch1 for the 7 feeds. The signal refers to the maximum counts (SARDARA) of 3C84 associated with the central beam while the noise corresponds to the rms of the maps.

Feeds	CH0	CH1
Feed 0	322487 / 902 = 357.5	301332 / 828 = 363.9
Feed 1	297208 / 721 = 412.2	291103 / 849 = 342.9
Feed 2	190665 / 328 = 581.3	244460 / 2853 = 85.7
Feed 3	197409 / 308 = 640.9	157740 / 896 = 176
Feed 4	168289 / 5248 = 32.1	281666 / 597 = 471.8
Feed 5	-	115791 / 255 = 454
Feed 6	202238 / 330 = 612.8	134912 / 765 = 176.4

Table 7: *Signal/Noise (max counts / rms) for Ch0 and Ch1 associated with the 7 feeds. The values correspond to the maps ra+dec of 3C84 obtained at 60°el on 17/12/2020. Channels with low Signal/noise due to the high noise are highlighted in red.*

1) Pointing models

Ideally, a new pointing model should be produced for each receiver (C, X and K-bands) at each change of season or at least once a year (during the winter season), and whenever a LUT updating is carried out in order to take into account the possible systematic pointing errors introduced by the new optical configuration.

Pointing models have been initially achieved for each SRT receiver (see Table 8; Bolli et al. 2015). Updating the models is important in order to check and improve the antenna pointing accuracy, in particular after major changes in the antenna (such as after the change of the actuators on the active surface, etc).
The strategy consists in performing OTF cross-scans in the horizontal frame on a large sample of pointing calibrators in order to cover the sky uniformly in azimuth and elevation. To sample also the most critical south-eastern and north-eastern quadrants, sources with dec > -45° and with flux > 1.5 Jy are selected (Tarchi et al. 2013; Ricci et al. 2016).
We measure for each cross-scan the pointing offsets. Observations are usually carried out during the night (avoiding sunrise and sunset) in order to minimize thermal effects on the structure, in particular at high frequency (K-band). Once the whole azimuth/elevation plane in the sky is correctly sampled (in general, observation sessions of at least 6 hours are required), we fit the data with a pointing model polynomial (Bolli et al. 2015) using pdplt, a tool part of the VLBI Field System.
The new pointing parameters are then implemented in DISCOS for the following testing session to improve and confirm the model. The solution is satisfactory once the azimuth and elevation residuals (i.e. pointing offset w.r.t. the source direction) in both the azimuth and elevation scans are lower than 1/10 of the beam size.
Several sessions are usually necessary in order to converge to an acceptable solution, in particular at higher frequency. Below we present the results in C, X and K-bands. More details of the analysis are presented in Appendix B.

	Observed center freq.	Pointing model residuals [arcsec]		
Rec.	[GHz]	σ_{az}	σ_{el}	Beam size [arcmin]
L	1.705	7	7	11.12
C	7.35	10.8	7.2	2.58
K	23	3.9	3.2	0.805

***Table 8**: Pointing model residuals and beam size for the different INAF receivers from Bolli et al. (2015).*

- **C-band**

The pointing model used during the recommissioning and until July 2021 was created on 04/12/2017 (mdlpo_C_2017335.ctl). It corresponds to the data acquisition performed on 30/11/2017 with the TP (LO=6800 MHz and BW=730 MHz). The model was then tested on 08/01/2018, confirming the satisfactory solution. The fit parameters of the model are reported in Table 9.

We acquired data on 02/09/2020 (session of 2 hours) in order to check the pointing model in C-band. We created an updated version of the model (mdlpo_C_2020069.ctl) then tested it by performing a session of pointing observations on 12/02/2021 (duration of 6 hours) using the TP (setLO=6200, bw=730 MHz, integration=40ms). The session allowed us to refine the pointing model, by creating a new pointing model (mdlpo_C_2021349.ctl). Indeed, it contains much more data and the flag of some outliers was more evident. However, we did not try this new pointing model because of the lack of time. The fit parameters are included in the last row of Table 9.

Model version	Mean and rms of the measured az- and el- offsets (°)	Fit parameters*				
00004 2012 346		-2.3029563427	0.0000000000	-0.0102762356	-0.0050985431	0.0008867322
		-0.0019946923	0.0873332769	0.0871561393	0.0000000000	0.0000000000
		0.0115426397	0.0000000000	0.0020223276	0.0008122203	0.0000000000
00005 2017 335 04/12/2017 mdlpo_C_2017335.ctl	Az-mean=+0.000440 Az-rms= +0.000790 El-mean= -0.001660 El-rms= +0.000910	-2.2957174778	0.0000000000	-0.0068070539	-0.0016828823	-0.0009974039
		-0.0006166724	0.0852021798	0.0925736725	0.0000000000	0.0000000000
		0.0148610147	0.0000000000	0.0005418550	-0.0000714987	0.0000000000
00006 2020 357 22/12/2020 mdlpo_C_2020069.ctl mdlpo_C_20200902.ctl (same file)	Az-mean= -0.001460 Az-rms= +0.001210 El-mean= +0.001440 El-rms= +0.001940	-2.2901301384	0.0000000000	-0.0017811353	-0.0001074947	-0.0011201684
		-0.0017191271	0.0922544748	0.0825878754	0.0000000000	0.0000000000
		0.0105356537	0.0000000000	0.0005174759	0.0004440407	0.0000000000
00007 2021 349 15/12/2021 mdlpo_C_2021349.ctl	check session not performed (rms residuals: Az-rms= +0.001410 El-rms= +0.001420)	-2.2939150333	0.0000000000	-0.0047341794	-0.0036865076	-0.0010470135
		-0.0018899474	0.0874233543	0.0871086046	0.0000000000	0.0000000000
		0.0158218201	0.0000000000	0.0001167601	-0.0001645046	0.0000000000

Table 9: *Updated versions of the pointing models in C-band. Values of the 1st and 7th parameters must be close between the version of a previous model compared to the updated one. The model created on 04/12/2017 (indicated in green) was used during the recommissioning and until July 2021. The last model updated on 15/12/2021 has not been tested. Mean and rms of the measured az- and el-offsets correspond to the successive check sessions. *The parameters are indicated in Orlati et al. 2016.*

- **X-band**

The observations dedicated to the realization of the pointing model for the right polarization at X-band were performed on the night between the 8 and 9 October 2020. The central frequency was set to 8450 MHz and we used the TP backend. Two couple of Az-El pointing cross-scans were performed continuously on a selected sample of radio source calibrators chosen among the list performed by Ricci et al. 2016 and with a flux density higher than 1.5 Jy.
For each cross-scan a coordinate offset is calculated, and a polynomial fit on all the data set of the session is executed through the pdplt software.
The implemented model was verified on 9 October 2020 and the resulting offsets respected the reference value of 1/10 of the HPBW. The parameters of the fit are indicated on Table 10.

Fit Parameters*				
-2.2955527306	0.0000000000	-0.0027078437	0.0173532944	-0.0008693041
-0.0019183123	0.1030814573	0.0856014490	0.0000000000	0.0000000000
0.0087973252	0.0000000000	0.0003481323	0.0001999680	0.0000000000

Table 10: *Parameters of the implemented version of the pointing model at X-band on DISCOS. *The parameter meaning is indicated in Orlati et al. (2016).*

- **K-band**

The K-band pointing model implemented in DISCOS from January 2014 until July 2021 is that of 2014 (mdlpo_K_2014010.ctl; Orlati et al. 2016). The model was performed at 22.36 GHz with the TP (LO=21900 MHz, BW=730, integration=40ms) during the technical commissioning. The span and scan speed were fixed at 0.3° and 0.8°/minute respectively, in order to obtain a sufficient number of samples per beam and to avoid losing tracking accuracy.

An attempt was made to create a new pointing model during the recommissioning. Five observations have been carried out in order to improve the model. The 5th observation was performed on 16/05/2018 (err2018.136). However, the fit was performed using the pointing model of 2012 (mdlpo.22GHz), which was used during the ESP, but apparently not implemented in DISCOS. This probably explains why it was not possible to find a satisfactory solution. Several trials were performed but the rms of the residuals were not lower than 1/10 of the beam size and some trends were still present in the data.

We acquired data on 18/09/2020 at 20.34 GHz with the TP (LO=19900, BW=730, integration=40ms), in order to improve the pointing model. We produced two versions of pointing models on 15/12/2021, but we did not have the time to refine them with additional sessions. The first model (err_2020_FEW_FLAGS.262) was obtained by flagging only 5 points (each point corresponds to one El+Az cross-scan) while the second one (err_2020_MANY_FLAGS.262) was produced by flagging 12 points. The model residuals indicate that flagging more points gives a better result, although we did not reach rms values lower than 1/10 of the beam. All the plots obtained during the data analysis of the data are in Appendix B. A summary of the different pointing model parameters is presented in Table 11.

Additional sessions during the night are required in order to refine the pointing model in K-band, based on err_2020_MANY_FLAGS.262. Thermal study of the structure of the antenna *(see Section 7)* using temperature sensors will be of utmost importance in order to compensate for the pointing model in K-band and at higher frequency (Attoli et al. 2022a; Attoli et al. 2022b).

Model version	Mean and rms of the measured az- and el- offsets (°)	Fit parameters*
0000X 2012 268		-2.2933666706 0.0000000000 -0.0081273140 -0.0185187403 -0.0013069536 -0.0009291506 0.3067421317 -0.2181605548 0.0000000000 0.0000000000 -0.0339095332 -0.0000435748 -0.0003875243 0.0004249602 0.0005932985 0.0002558492 0.0002624479 0.0001502736 0.0016966705 -0.0025470885
00000 2014 010 mdlpo_K_2014010.ctl	Az-rms= 0.0011 El-rms= 0.0009	-2.2964186668 0.0000000000 -0.0061030770 -0.0035287447 -0.0014408963 -0.0017973853 0.0719125122 0.0925239921 0.0000000000 0.0000000000 0.0128885703 0.0000000000 0.0006690503 0.0000107827 0.0000000000
00006 2018 137 err2018.136 (recommissioning)	Az-mean= 0.000850 Az-rms= 0.000870 El-mean= -0.001280 El-rms= +0.001200	-2.2947800159 0.0000000000 -0.0049467222 -0.0005438862 -0.0003827636 -0.0001526908 0.0958994329 0.0848703235 0.0000000000 0.0000000000 0.0054536290 0.0000000000 -0.0001463571 -0.0000076018 0.0000000000
00001 2021 349	check session not performed	-2.2947826385 0.0000000000 -0.0044269077 -0.0017407239 -0.0010548742

err_2020_FEW_FLAGS.262	(rms residuals: Az-rms= +0.001350 El-rms= +0.002010)	-0.0019802644 0.0681823194 0.0933056250 0.0000000000 0.0000000000 0.0142154460 0.0000000000 0.0002206409 0.0001436503 0.0000000000
00001 2021 349 err_2020_MANY_FLAGS.262	check session not performed (rms residuals: Az-rms= +0.001210 El-rms= +0.001700)	-2.2955031394 0.0000000000 -0.0054976767 -0.0029845607 -0.0011973275 -0.0020347356 0.0673265010 0.0942032337 0.0000000000 0.0000000000 0.0146043756 0.0000000000 0.0000240032 0.0003345838 0.0000000000

Table 11: *Updated versions of the K-band pointing models. The pointing model implemented in Discos is that of 2014 (indicated in green). The last model has to be refined in order to reach an acceptable value of the rms. *The parameters are indicated in Orlati et al. 2016.*

2) Focus

The focus of the telescope has to be kept under control since temperature gradients or other atmospheric effects can degrade its stability, which could have direct effects on the quality of the data. The calibrators used to correct the focus parameters of the antenna need to have the same characteristics as those used for pointing (see previous section).

Below we report the measurements performed during the recommissioning related to the focus in C- and K-bands. We did not perform measurements in 2020.

Note that in order to evaluate the correct focal position, the scan length has to be three times the wavelength of observation. The maximum excursion permitted along the focal axis is 150mm. For this reason, the focus measurements cannot be performed at L and P band (the scan length would be 600 and 3000 mm, respectively). Therefore the values adopted for the L-band are the same as in Bolli et al. (2015).

- **C-band:**

A focus curve was successfully obtained during the recommissioning on 31/01/2018 (Fig. 18) by alternating pointing and focus scans (0.5°, speed 3°/min, duration of scan ~1min, HOR frame) on 3C48 in the 78°-13° elevation range. The test was carried out using the TP, with setLO=6800 MHz and bw=730 MHz.

The curve was correctly fitted with a polynomial of degree 6 as reported below (Table 12) .

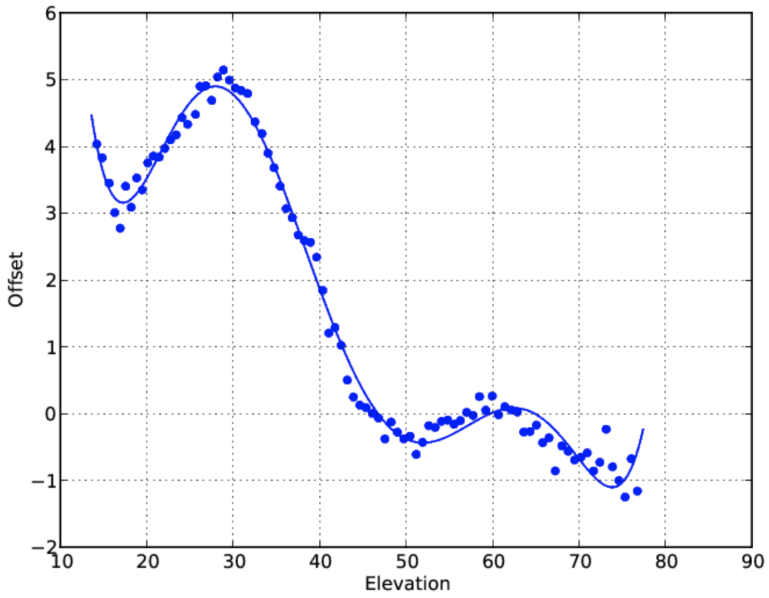

Figure 23: *Focus curve obtained in C-band during the recommissioning on 31/01/2018.*

We fit the curve with a polynomial of degree 6, such as:
y=ax^6+bx^5+cx^4+dx^3+ex^2+fx+g

Parameters	Values
a	2.36410838911e-08
b	-6.62393455442e-06
c	0.000733782714288
d	-0.040640240455
e	1.16941963489
f	-16.4202062811
g	91.5590595452

Table 12: *Parameters of the fit associated to the focus curve in C-band.*

- **X-band:**

We carried out the observation to produce the focus curve using the TP backend with a bandwidth of 28 MHz (ASI downconversion) on 19 October 2020 from 16:44 to 23:56 UTC. We selected the right polarization and the central frequency was set to 8450 MHz. The procedure was to follow the radio source calibrator 3C84 from about 5° to 80° of elevation, continuously performing 4 pointing cross-scans (0.5°, speed 3°/min, HOR frame) and one focus-scan (z-axis span 150 mm, duration 60 s). The result is shown in Fig. 24.

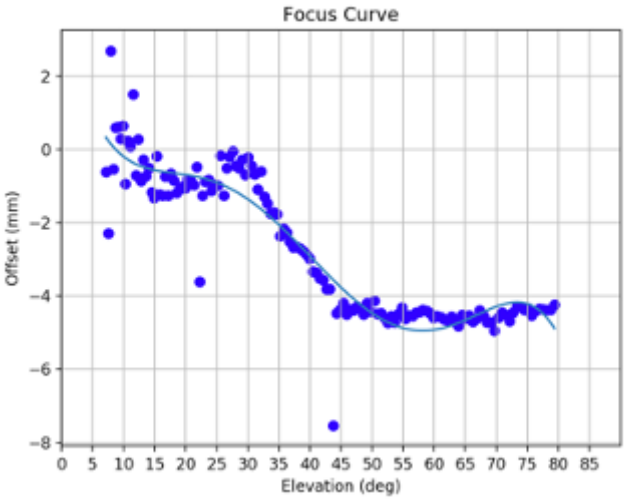

Figure 24: *Focus curve obtained in X-band.*

We fit the curve with a 5th degree polynomial function:

y=a*x^5+b*x^4+c*x^3+d*x^2+e*x+f

To be investigated whether the 6th degree polynomial fit gives better results.

The parameters resulting from the fit are shown in Table 13.

Parameter	Value
a	-1.1325543951e-07
b	2.36150814917e-05
c	-0.00174391217523
d	0.0549219553414
e	-0.79549230785
f	3.78481445013

Table 13: *Fit parameters resulting from the focus curve obtained at X-band.*

- **K-band:**

A session dedicated to the focus on 3C286, 3C345 in the 8°-87° elevation range was performed on 12/06/2018 (LO=23000 MHz, bw=730 MHz). We alternated pointing and focus scans. The focus curve is presented in Fig. 25, together with the previous focus data. An anomalous behavior was noted below 35°, causing a severe defocusing. The weather conditions were clear and no particularly relevant RFI was recorded in the observation log. However the report mentions quite large pointing errors that might affect our measurements. Because of the anomalous behavior, the old focus curve implemented in DISCOS (previously called Nuraghe) on 14 January 2014 was maintained.

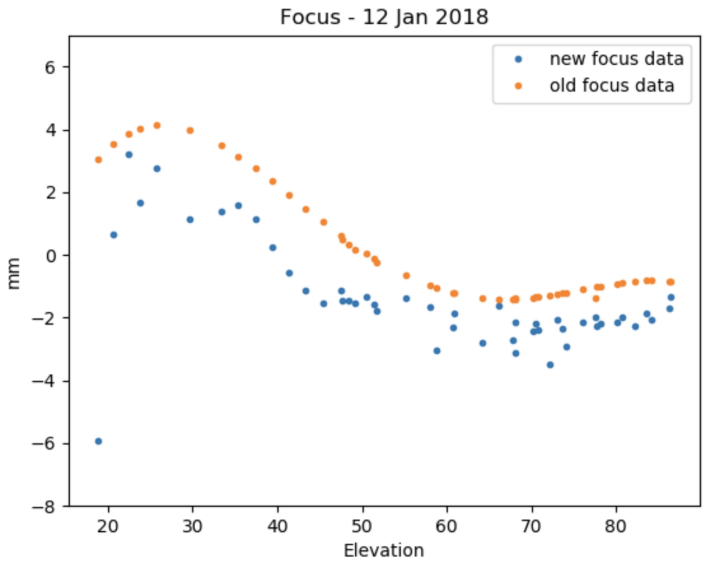

Figure 25: *Focus curves at K-band obtained during the recommissioning (blue dots) and previously (14/01/2014).*

3) Gain curves

In the following, we report the gain curves (gain versus elevation) associated with the C, X and K-bands.

From the measured gain curves (gain vs. elevation), one fits a 2-degree polynomial with the parameters C0, C1 and C2:

$$\text{gain [K/Jy]} = C2\ El^2 + C1\ El + C0$$

We did not perform new measurements in C-band in 2020, we only report the results obtained during the recommissioning. In the case of the L-band receiver, we did not carry out sessions dedicated to the pointing, focus and gain curves. The values adopted are those reported in Bolli et al. (2015).

The K-band gain curves were obtained by using the M1-LUT and the *"new M1-LUT",* during the recommissioning (2018) and in 2020, respectively. We performed the analysis with the SCUBE software (Murgia et al. 2016).

- C-band

C-band gain curves were performed during the recommissioning on 18 and 24 January 2018 at 7.3 GHz (Fig. 26 and Table 14), using the same frequency and bandwidth as mentioned in Murgia et al. (2016). The results are consistent. However, we obtained a gain of 0.69 K/Jy at 45°el, which is 10% higher than that of Murgia et al. (2016), 0.63 K/Jy (averaging the two polarizations). We note that our measurements were obtained with cross scan, while Murgia et al. used OTF maps. In addition, we used the 2012 value of the flux density of 3C147. However, its flux density was found to be slightly variable and has increased in the last few years. Using the most recent value (January 2016, see the JVLA website), the measured gain at 45° decreases to 0.66 K/Jy, which is closer to the value found by Murgia et al. (2016) and is consistent with the theoretical value (e.g. Bolli et al. 2015).

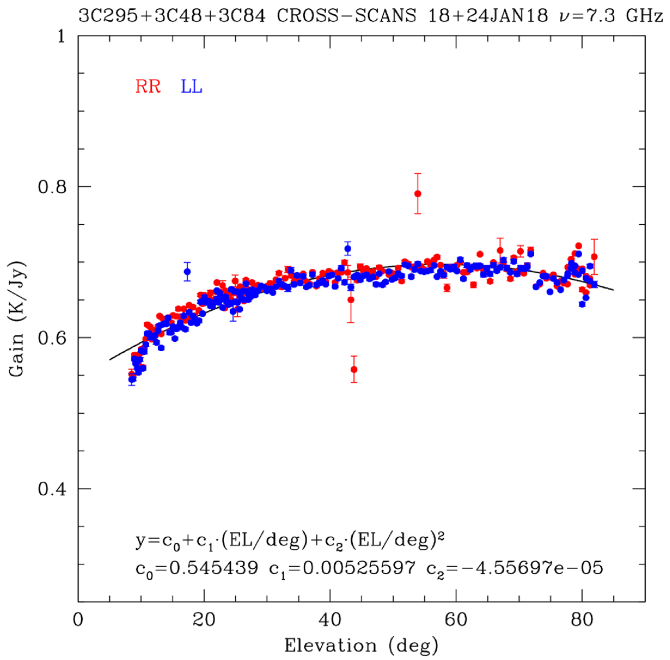

Figure 26: *Gain curves obtained at 7.3 GHz based on the data collected on 18 and 24 January 2018.*

Parameters	Values
C0	0.545439
C1	0.00525597
C2	-4.55697e-5

Table 14: *Parameters of the 2-degree polynomial fit associated with the C-band gain curve obtained in 2018.*

- **X-band**

A dedicated experiment was carried out on 23 March 2021 in order to measure two orthogonal cuts (cross-scan) of the SDSA far-field pattern at 8.45 GHz and compare it to the GRASP simulation. In Figure 27 we present a normalized radiation pattern of the SDSA illuminated with the X-band feed horn at 8.45 GHz at 66 deg of elevation. An integration time of 40 ms was set in the total power backend with a bandwidth of 28 MHz centered at 8.45 GHz

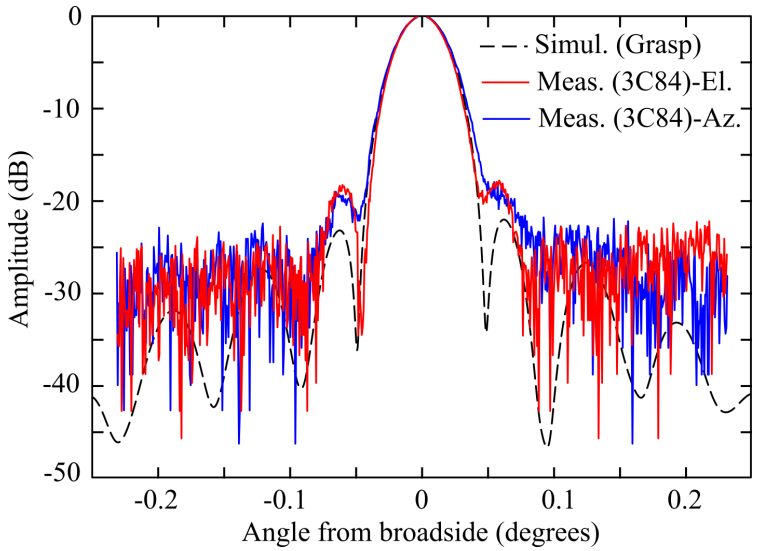

Figure 27: *Normalized radiation pattern of the SDSA at 8.45 GHz: comparison between the GRASP simulation and the orthogonal (azimuthal and elevation) cuts measured by performing cross-scan of 0.5° length on 3C84.*

Ratio G/T has been computed by selecting the radio calibrator source 3C147 on 3 February 2021 (Fig. 28). Specifically, its flux density value is evaluated to be 4.68±0.05 Jy at 8.45 GHz. We tracked the calibrator source from an elevation angle of 80° to the minimum elevation available for the SRT (about 6°), measuring both the power from the cold sky and the additional power from the calibrator. An integration time of 40 ms was set in the total power backend with a bandwidth of 28 MHz centered at 8.45 GHz.

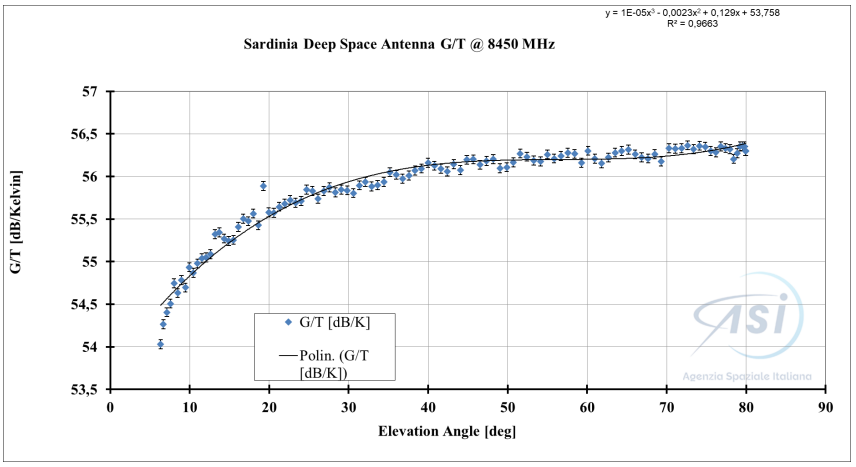

Figure 28: *Antenna Gain Curve G/T (power gain-to-system noise temperature ratio).*

During the same measurements, we used the noise source and we reported the gain curve in K/Jy (DPFU) in Fig. 29.

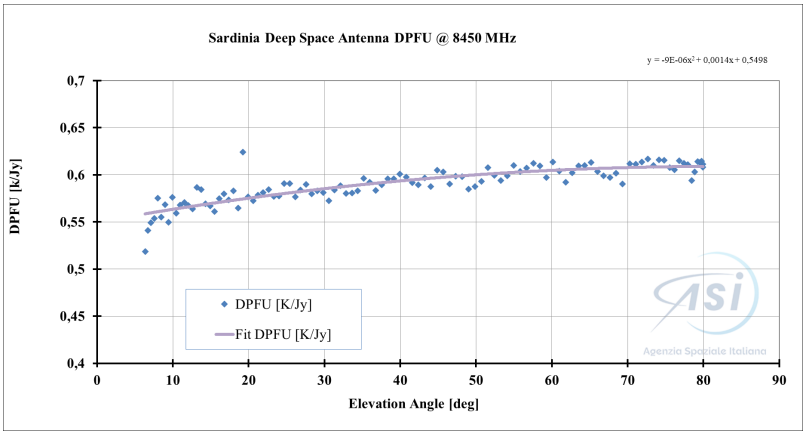

Figure 29: *Antenna Gain Curve DPFU (degrees per flux density unit).*

From the same data set, we measured beam deformation of the SDSA illuminated with the X-band feed horn at 8.45 GHz (Fig. 30). The red line is the linear fit of measured data.
The measured half power beamwidth (HPBW) is in good agreement with simulations that reports the measured beam deformation and with respect to the simulated HPBW at different elevation angles, defined as:

$$\varepsilon = \sqrt{(\theta_{\mathrm{az}} - \theta_e)^2 + (\theta_{\mathrm{el}} - \theta_e)^2}$$

where θ_az and θ_el are, respectively, the HPBWs measured along the azimuth and elevation axis using the calibrator radio.

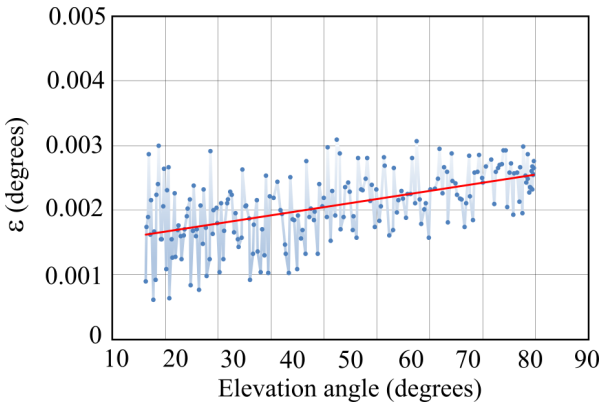

Figure 30: *Measured beam deformation using the cross-scan.*

- **K-band**

We report the gain curves obtained at 20.3 GHz (central frequency) associated with the central feed using the M1-LUT created in 2012 and the *"new M1-LUT"* produced in dedicated OOF holography measurements performed at 22.23 GHz in the elevation range 20-70° (Buffa et al. 2020). The observing strategy consists in performing repeated pointing and cross-scans on 3C286 from 20 to 80° el using the TP (setLO=19900, bw=730 MHz, integration=40 ms). Note that gain curves obtained for the central feed are also consistent with that of the lateral feeds (Murgia et al. in prep). Observations

using the old M1-LUT were performed on 9 September 2020. We employed the new M1-LUT, instead, in the set up of the observations taken on 29 September and 17 December 2020.

We present in Fig. 31 *(left)* the gain curve obtained with the M1-LUT using data collected on 9 September 2020. It was obtained by fitting simultaneously the RR and LL measurements in the 20-80° elevation range. The opacity, as measured by means of skydip scans, was tau=0.44 during the session. The gain peak reaches 0.56 K/Jy at 66° of elevation. This value is comparable with the previous session performed on 22 February 2019 (peak gain of 0.53 K/Jy; Fig. 31 *(right)*), but still lower than the standard tabulated value of 0.66 K/Jy.
The high and quite puzzling value of the opacity might be responsible for this difference**.** Indeed, the value of the opacity is not consistent with that provided by the radiometer (0.09-0.1 over all the duration of the observing session). However, we prefer to adopt this value since it is derived through skydips and therefore more representative of the observing conditions (e.g. in case of condensation in the antenna cover).

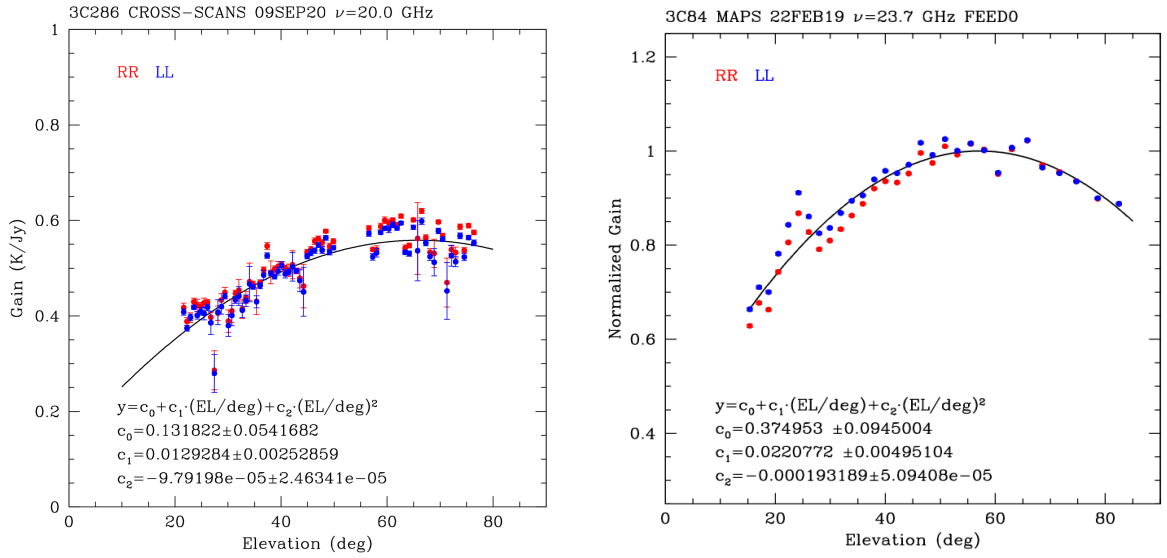

Figure 31: *Gain curves obtained with the old LUT based on the data collected on 9 September 2020 from 07:54-14:28 UTC (left) with an opacity tau=0.44 (fit of the skydip), and obtained on 22 February 2019 (right).*

Parameters	Values
C0	0.131822
C1	0.0129284
C2	-9.79198e-5

Table 15: *Parameters of the 2-degree polynomial fit associated with the K-band gain curve obtained in Sept 2020 with the old LUT.*

The gain curve obtained from the data collected on 29/09/2020 (see Fig. 32) is consistent with that using the M1-LUT, with the gain peak of 0.56 K/Jy reached at 66° of elevation. However, we need to repeat the test with the “new M1-LUT” covering all the elevations (in particular the low elevations) in order to understand if the “new M1-LUT” improves the gain curve.

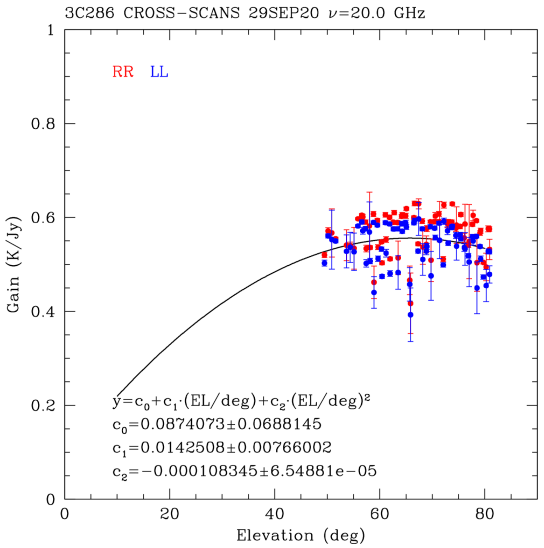

Figure 32: *Gain curves using the new M1 LUT obtained from the data collected on 29/09/2020 from 09:03-14:56 UTC.*

We expect significant improvements at lower elevation (below 45°) where the optics alignment gets worse (above 45° the optics alignment is quite good). More tests on the whole elevation angular range are needed to appreciate possible improvements and draw conclusions.

4) Radio Sun observations as a probe of dynamic range

Due to its very high signal, Sun observations can represent a suitable tool for testing/monitoring instrumental response (e.g. dynamic range and flux calibration) in the future, even in case of non-optimal observing conditions (e.g. high sky opacity) and/or when using high-frequency receivers. On the other hand, anomalies in the quiet-Sun (QS) level in K-band (probably due to RFI contaminations, ripples and/or LNA instabilities) were detected in a few SRT solar sessions in 2021, needing further investigations.

SRT is enabled to perform solar observations in K-band after the implementation of a dedicated instrumental and data analysis setup developed through the SunDish project (see https://sites.google.com/inaf.it/sundish and references therein for technical details).
Solar imaging observations at SRT require a special hardware configuration in order to attenuate the strong solar signal in the amplification chain: a manual setup of additional hardware (10 dB attenuation for the 14 multi-feed chains, 7 for each polarization section) is required at each solar observing session.

OTF scans provide full solar mapping, spanning the region on and around the Sun, covered by all the 7 feeds of the receiver, along the RA direction. In the above-mentioned receiver configuration, the SARDARA spectro-polarimeter allows us to detect both the bright solar disk (chromospheric emission) and the weaker emission near the limb, in the same image. Maps with SRT were performed at 18.8 GHz and 24.7 GHz (after a specific test phase, we decreased the frequency from the initial 25.5 GHz to match better receiver performances and avoid RFI), near the edge of the K-band in order to minimize errors in spectral index measurements. SARDARA setup usually requires the full 15-dB signal attenuation for the 4 first channels at the back-end level for optimal solar observations.

Accurate calibration adopting the Supernova Remnant Cas A as a flux reference, provided typical errors < 3% for the estimation of the QS components and for active regions flux measurements. The sensitivity of our solar images is calculated through the measurement of the background

brightness temperature fluctuations in map regions far from solar disk emission. Image sensitivities (RMS) are typically in the range 0.1–0.3 K for SRT.

We measured a quiet-Sun brightness temperature of about 10,000 K in the 18-26 GHz frequency range, a result in agreement with literature values within errors (a few percent discrepancies using 2018-2020 SRT data). This proves that our high-flux solar measurements determined a linear response from the system. Therefore, we can claim a (calibrated) signal-to-noise ratio for the QS emission of about 10^5.

5) Thermal study of the structure of the antenna

Thermal study of the structure of the antenna using temperature sensors will be of utmost importance in order to apply proper corrections to the pointing models at high frequency (Attoli et al. 2022a; Attoli et al. 2022b).

Thermal loads that occur throughout the antenna, e.g. due to exposure to solar radiation, can generate structural distortions that affect its performance. Using a numerical approach based on the Finite Element Method (FEM), a sensitivity analysis was performed in order to identify which components most influence the pointing of SRT when thermally stressed.
The observed direction is idealized through a vector shown in Fig. 33, called the Pointing Vector. To define the pointing vector, the presence of the secondary mirror has been neglected as its position is corrected by actuators following the indications in the dedicated Lookup Table.

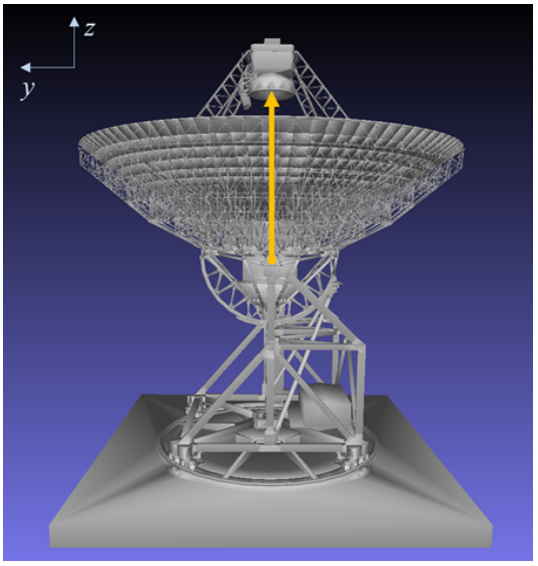

Figure 33: *Theoretical pointing vector of SRT when the antenna is at an elevation angle of 90 °.*

Therefore, a thermal load of 10°C was applied iteratively to each element of the model; hence, the pointing error that it produces was estimated through the Pointing Vector Rotation (PVR) parameter defined by the relation:

$$PVR = \sqrt[2]{(\varphi_x)^2 + (\varphi_y)^2 + (\varphi_z)^2}$$

in which φ_x, φ_y and φ_z are the rotations of the pointing vector with respect to the ideal direction.

Fig. 34 shows, through a gradation of colors, the magnitude of the pointing error produced by each element belonging to the four main macro-components listed in a bottom-up sequence.

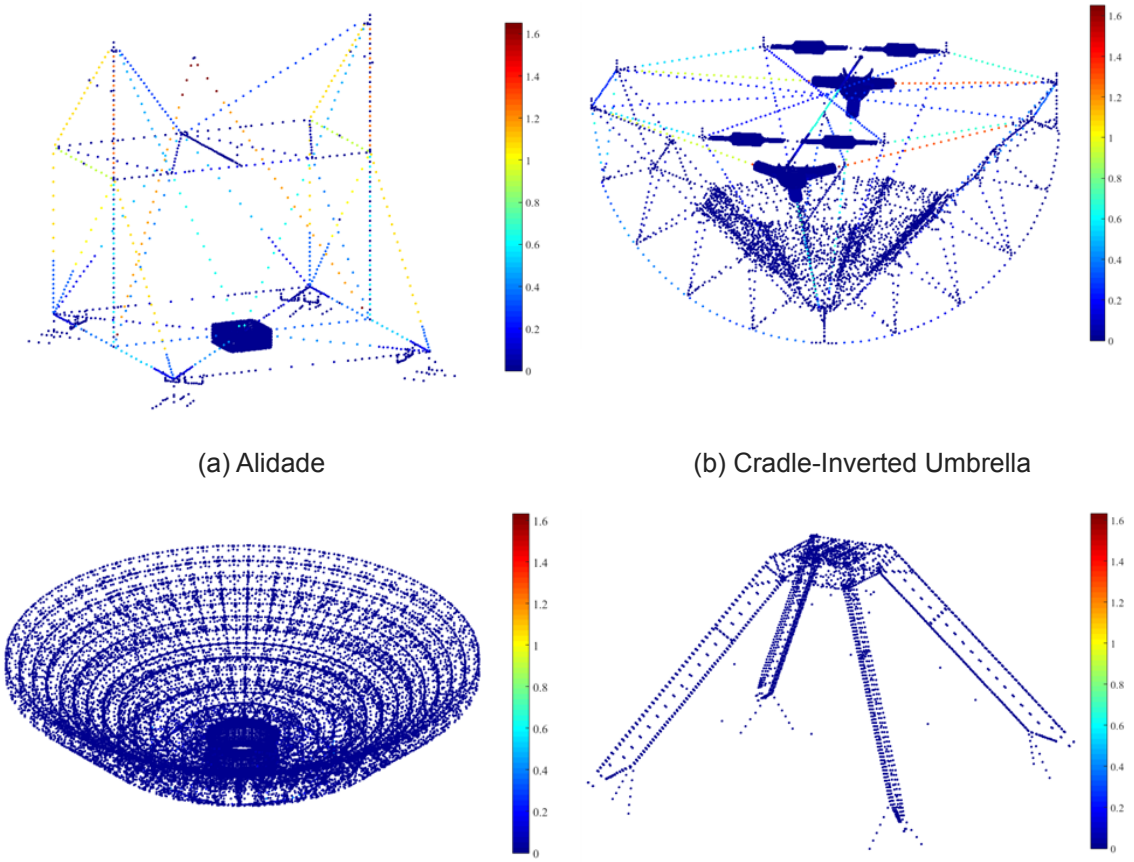

(a) Alidade

(b) Cradle-Inverted Umbrella

(c) Back Up Structure

(d) Quadrupod

Figure 34: *Map of the influence on the pointing of each element of the finite element model with elevation angle equal to 90 deg. Each point on the map represents an element and the color gradation expresses the PVR value (in arcsec) it produces.*

The study showed that the Alidade and the Cradle-Inverted Umbrella system are the most thermally critical macro-components. The sensitivity analysis also makes it possible to identify which elements need more precise thermal characterisation by means of a higher number of thermocouples.
Fig.34 (c) shows that the thermal stress of the Back Up Structure (BUS) does not generate important effects on the pointing. However, it is interesting to analyze the consequences on the accuracy of the main reflector surface.

Simplified scenarios with different heating conditions were generated (see Fig. 35) focusing on two tilt angles: 80° and 30°. The two positions can be considered as the extremes of the SRT operating range. In order to calculate the displacements undergone by the main mirror in the direction orthogonal to the surface with respect to the ideal shape of the paraboloid (also called deflections), simulated temperatures were applied to the Finite Element model.

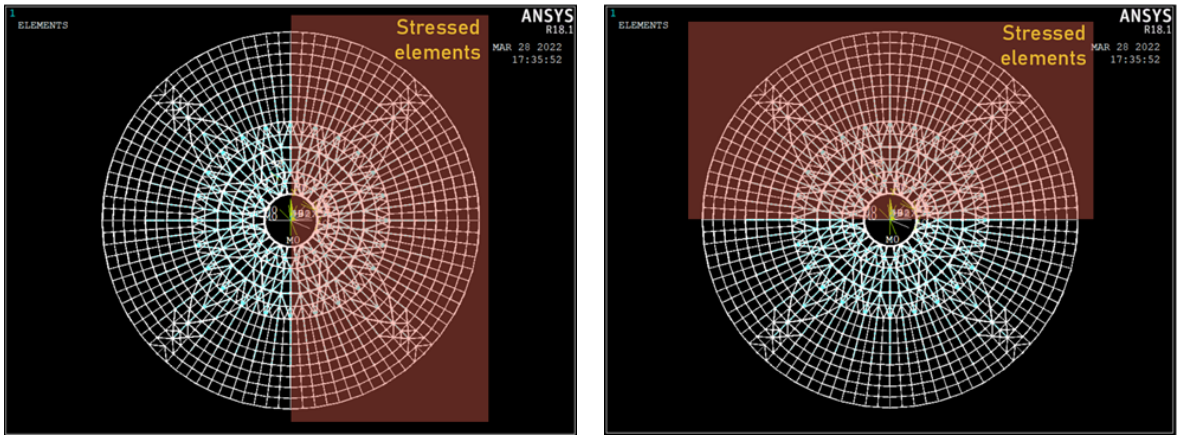

(a) Thermal load applied on right side elements (positive x).

(b) Thermal load applied on front side elements (positive y).

Figure 35: *Identification of the stressed elements in the two thermal load application cases. A thermal load of 5°C was applied to the elements highlighted in red. The choice of the value is due to the magnitude of the thermal gradients between the sunny and shady sides found in thermographic images.*

The study made it possible to quantify the effects due to the thermal load (Fig. 36), and to compare them with the deflections produced by the gravitational action (Fig. 37). Then, the consequences generated by the concomitance of the two stresses were evaluated (Fig. 38-39).

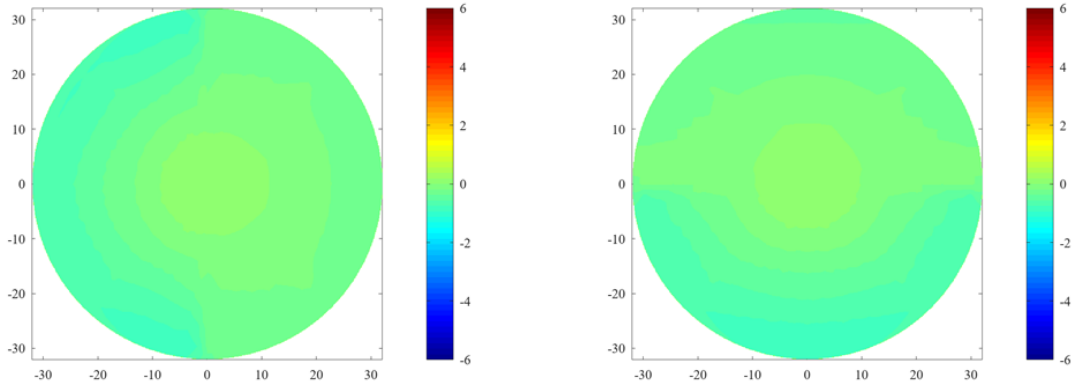

(a) Thermal load applied on right side elements.

(b) Thermal load applied on front side elements.

Figure 36: *Main reflector deflections map (in mm) due to only thermal stress. The two maps correspond to the load configurations, (a) and (b), presented in Fig. 35.*

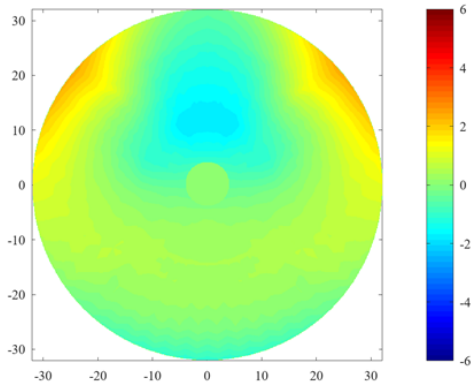

(a) Elevation angle equal to 30°.

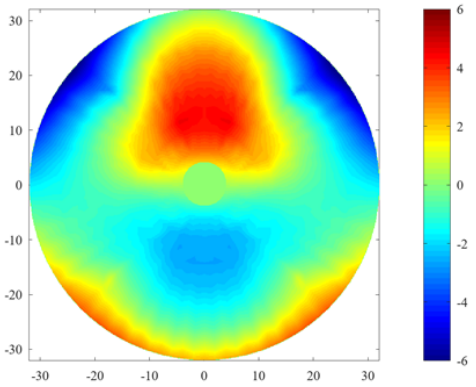

(b) Elevation angle equal to 80°.

Figure 37: *Main reflector deflections map (in mm) generated by the gravity force affecting the structure at the two elevations considered.*

The maps make it clear how much the deflections produced by gravitational action prevail over the deflections generated by thermal stress. This is also evidenced by the rms values shown in Table 16.

Gravitational Load			**Thermal load**		
Elevation [DEG]	30	80	Heated side	Front side	Right side
rms [mm]	0.812	2.071	*rms* [mm]	0.249	0.248

Table 16: *Estimated rms value by applying to the FE model first only the gravitational load (on the left), then only the thermal load (on the right).*

However, at high frequencies, such accuracy is required so that thermal effects cannot be neglected. The maps in Fig. 38-39 show the orthogonal displacements to the main reflector surface due to the simultaneous action of gravity and thermal load for elevation angles 30° and 80°; Table 17 shows the rms values achieved in the same combinations described.

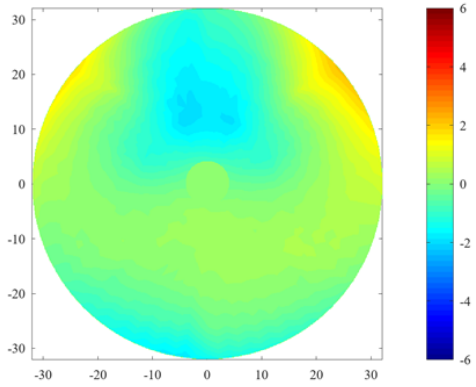

(a) Thermal load applied on right side elements.

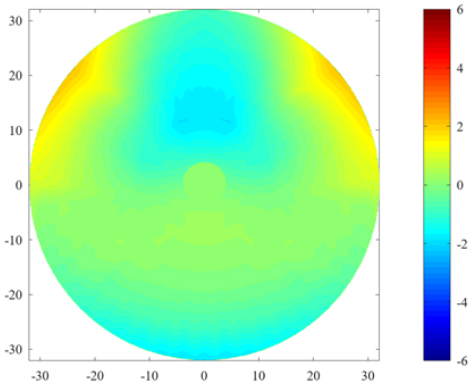

(b) Thermal load applied on front side elements.

Figure 38: *Main reflector deflections map (in mm) produced by the concomitant action of gravitational and thermal loading when the antenna observes at an elevation angle of 30°.*

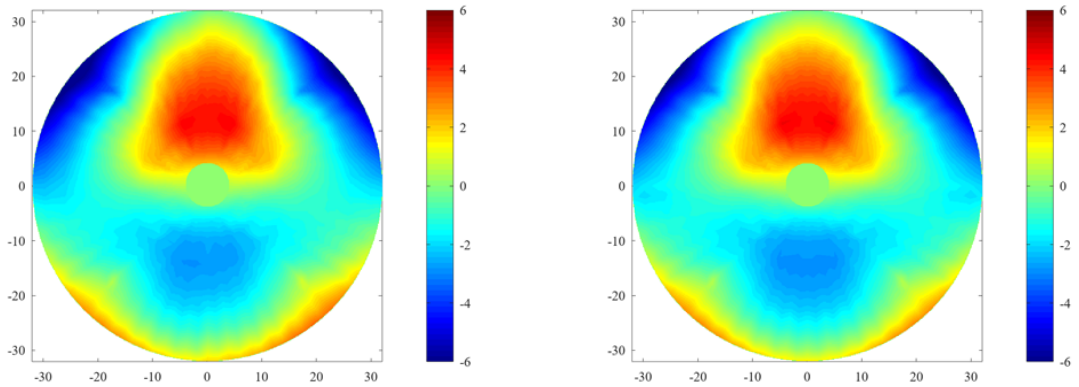

(a) Thermal load applied on right side elements. (b) Thermal load applied on front side elements.

Figure 39: *Main reflector deflections map (in mm) produced by the concomitant action of gravitational and thermal loading when the antenna observes at an elevation angle of 80°.*

Elevation [DEG]	30	80
Front side	0.809	2.087
Right side	0.772	2.123

Table 17: *Estimated rms value by simultaneously applying both the gravity load and the thermal load to the FE model.*

It can be seen that as the tilt angle increases, the optical coma phenomenon related to the gravitational effect becomes more pronounced. This could be caused by the lack of structural symmetry in the elevation wheel truss system. Nevertheless, it is important to point out that the deflections suffered by the main mirror due to gravitational loads are compensated. This is performed by means of actuators that correct the shape of the SRT active surface. The elongations or contractions of the actuators are defined through Lookup Table (LUT).

6) Conclusions

Characterization tests were performed in L, C, X and K-bands from September 2020 to February 2021 in order to verify the correct functioning of the different components after a long stop of the antenna in 2020, and possibly improve the observing performances at the different frequencies. We provided measurements of the beam shape, pointing, focus and gain curves for the different receivers and compared them with those carried out during the recommissioning in 2018.

Such measurements were performed first by setting the active surface in the ordinary configuration, i.e. setting the current M1 LUT, and then replacing the latter with a new M1-LUT derived by more recent OOF holography measurements. The tests show very similar results between 2018 and 2021 for the different receivers, which shows that the stability of the antenna components and the antenna performances did not change after the antenna downtime.

The beam size and beam deformations obtained in C and K-bands appear consistent with the measurements reported during the AV and the technical commissioning. The beam shape is mostly consistent with the theoretical value around 60° of elevation, as expected from the actual SRT best performances at these elevations. The secondary lobes still appear strongly asymmetric in particular at low elevations (below 30°el), as already noticed during the AV.
The experiment with the new M1-LUT, aimed at correcting for these residual large scale optical aberrations by moving the M1 actuators, produced incomplete results and no conclusions can be drawn. We are waiting for the correction of these aberrations by means of a fine calibration of the M2-LUT (as planned after the installation of the new metrology system). In any case, it is still worth it to schedule this kind of experiment again in order to fully investigate the active surface's potential.

We tried to improve the pointing models in C and K-band. Additional sessions are necessary in order to test the new pointing model in C-band and refine the K-band model. The pointing performance in K-band will be highly improved by providing a fine calibration of the M2-LUT and will definitely take advantage of the metrological systems. These improvements represent a key objective of the PON in order to be able to observe at up to 115 GHz (Navarrini et al. 2022; D'Alessandro et al. 2022).

The characterization of the SDSA X-band receiver shows good performances in terms of gain curve and pointing accuracy at least around 8.45 GHz. These performances are also in good agreement with those of the C-band receiver hosted in the other BWG focus.

7) Notes for the next tests

- **General notes:** We could use the TP instead of SARDARA to perform most of the tests in C and K-bands (if the RFI are not disturbing the band). Check the integration time for the different tests. We have to dedicate more time to the tests in order to have wider statistics and reduce the time between the analysis of the data and the observations.

- **C-band pointing model:** sessions of at least 6 hours to have a good statics and full coverage in Az and El (select more calibrators at high elevation (> 80°el)?

- **K-band pointing model:** more sessions in order to refine the model and reduce the pointing offsets in azimuth and elevation to less than 1/10 of the beam size. Sessions have to be performed during perfect weather conditions. It would be useful to add calibrators at low and high elevations to better understand the trends and the outliers (< 10/20° and >80/85° el : data can be considered as outliers). It is necessary to perform the test during the night to avoid thermal variations of the structure and to repeat the session several times to improve the model at each session. Ideally, a new pointing model should be produced at least every year (during the winter season), with the creation of a new LUT in order to improve the new version of the pointing model. The last pointing model was performed at 20.3 GHz. The best strategy would be to perform several sessions during the night at the highest frequency (25-26 GHz), with a very good coverage at low elevations but be sure of the good and stable

response of the receiver at this frequency. Otherwise, we could perform the pointing model at 3 different frequencies (low, mid, high) in the K-band since the beam size changes in a significant way between 18 and 26 GHz. Then the sessions have to be repeated during the day in order to check the corrections of the M1 LUT.
In order to optimize the pointing sessions and save time, check the website: https://xephem.github.io/XEphem/Site/xephem.html. It allows us to download catalogs of pointing sources and schedule the observations w.r.t. their position in the sky w.r.t. SRT.

- **Gain curves:** Repeat gain curve measurements at K-band with the new M1-LUT. Compare our observative strategy with the ITU measurement technique (technique used by the ASI team for the X-band receiver). Pay attention to the value of the noise source and its tolerance at high frequency (25-26 GHz). Check periodically the gain curves of lateral feeds in K-band (map technique). It would be also useful to have gain curves at different frequencies for the 7 feeds. Check the values of the calibration marks, measuring them with respect to flux calibrators (e.g. planets), especially for the K band (at Medicina, the values of the calibration mark between 18 and 19 GHz are poorly realistic). Check the feasibility of using planets as calibrators, e.g. Uranus and Neptune (check the visibility with NASA-Horizons).

- **Beam shape:** Perform some cross-scans at different elevations in addition to the maps on 3C84 with a small but adequate sampling time (low antenna velocity, 100ms?) in order to compare the scan profiles (in particular the secondary lobes) with the simulations (Nesti's model). CS and OTF maps on 3C84 give complementary information. **In K-band**: check the beam shape at 18.7 and 24.5 GHz, add skydip, more calibrators and maps on other calibrators (in addition to 3C84) at 20-30° and 30-40° el in order to better understand the flux contribution in the secondary lobes, more passages/beam (6 instead of 4: see maps in L-band).

- **Stability of the K-band receiver:** check the stability at 25-26 GHz and the contribution of the secondary lobes.

- **X-band receiver:** Despite characterization of the X-band receiver shows good performances, we expect that the side lobe level w.r.t. the main beam maximum at the X-band may be a little bit reduced, approaching the design requirement (< -20 dB), by a fine adjustment of the M3-M5 reflectors alignment. Therefore, we propose to perform new tests to find out the proper M3-M5 alignment which minimizes the side lobe level.

Appendix A: Beam shape

	C-band	K-band
Map size	0.5°x0.5°	0.2°x0.2°
Number of subscans per beam	5	3
Antenna speed	3 arcmin/s	6 arcmin/s
Coordinate frame	HOR	HOR
Backend	Total Power	Total Power
LO (MHz)	6800	21535
bandwidth (MHz)	680	680
Integration time (ms)	40	15
SRT Surface	Shape	Shape

Table A.1 : *Observation parameters used during the recommissioning.*

	L-band	C-band	K-band
Map size (deg)	2°x2°	0.5°x0.5°	0.2°x0.2°
Beam size (arcmin)	14.2 @1.4 GHz	2.71	1
Number of subscans per beam	4 (A) 8 (B)	4	4
Antenna speed (arcmin/s)	3 (A) 5 (B)	5	6
Coordinate frame	HOR	HOR	HOR
Backend	Sardara	Sardara	Sardara
LO (MHz)	-*	6200	17900
bandwidth (MHz)	500**	1500	1500
Integration time (ms)	15	20	15
Receivers Mode	XXL4		
Set Section Sardara	0,*,1000,*,*,2000, 16384	*(default: bw=1500, 1024 channels)*	*(default: bw=1500, 1024 channels)*
SRT Surface	Parabolic	Shape	Shape

Table A.2: *Details of the schedule and Saradara parameters used for the tests performed from September to December 2020. (A) and (B) correspond to the 15/09/2020 and 03/11/2020 sessions, respectively. (*): LO= 2300 is necessary for the TP, but not for Sardara. (**): Effective bandwidth since the XXL4 filter has a bandpass of 1300-1800 MHz.*

	L-band	C-band	K-band
Sessions	15/09/2020 (A) 03/11/2020 (B)	29/09/2020 (A) 07/11/2020 (B)	14/09/2020 (A) 16/12/2020 (B) 17/12/2020 (C) 18/12/2020
Target	CygA-Az (A) CygA-El CygA-Az (B) CygA-El	3C84-Az x 2 (A) 3C84-El 3C84-Az x 10 (B) 3C84-El x 10	3C84-Az x 6 (A) 3C84-El x 5 3C84-Az x 7 (B) 3C84-El x 5 3C84-Az x 11 (C) 3C84-El x 9
Elevation ranges	23-35° (A) 54-73° (B)	26-20° (A) 25-80° (B)	45-20° (A) ? 40-77° (B) 49-80 & 80-15° (C)
Calibrators	3C147 CS (A) 3C295 CS (B)	3C286 CS (A) 3C48 CS x 3 (B)	3C147 CS (B) 3C147-Az 3C147-El 3C147 CS x 3 (C) 3C147-Az x 3 3C147-El x 2
Weather		very cloudy (A) clear (B)	cloudy (B) clear then foggy(C)

Table A.3: *Summary of the observations performed from September 2020 to December 2020 for the different receivers. Note that the new M1-LUT was used for the sessions B) and C) in K-band.*

Appendix B: Pointing model

Plots obtained with pdplt for the different sessions.

1) Pointing model in C-band

A) Creation of a new pointing model on 04/12/2017 (mdlpo_C_2017335.ctl) based on the observations performed on 30/11/2017.

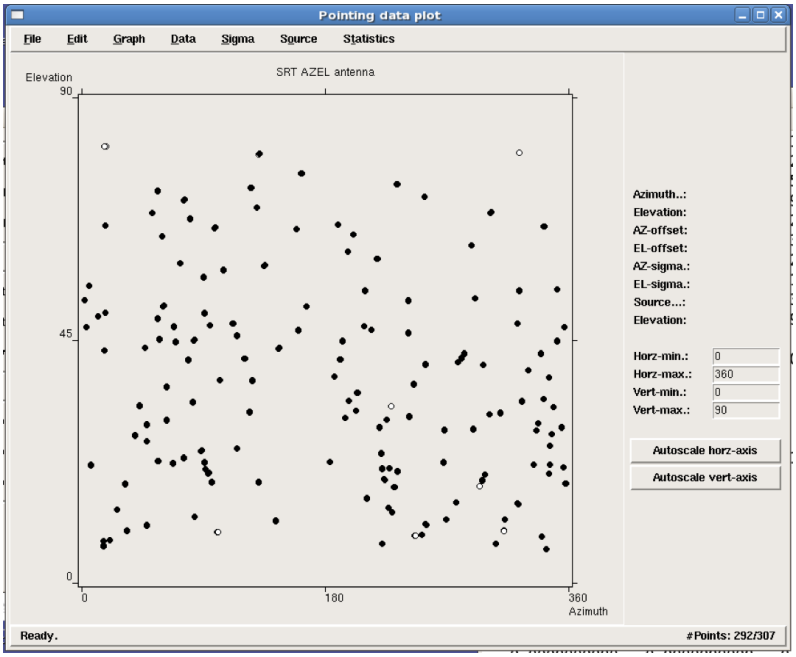

***Figure B.1**: Az-El coverage of the datasets consisting of 307 points (each point represents an Az/El cross-scan).*

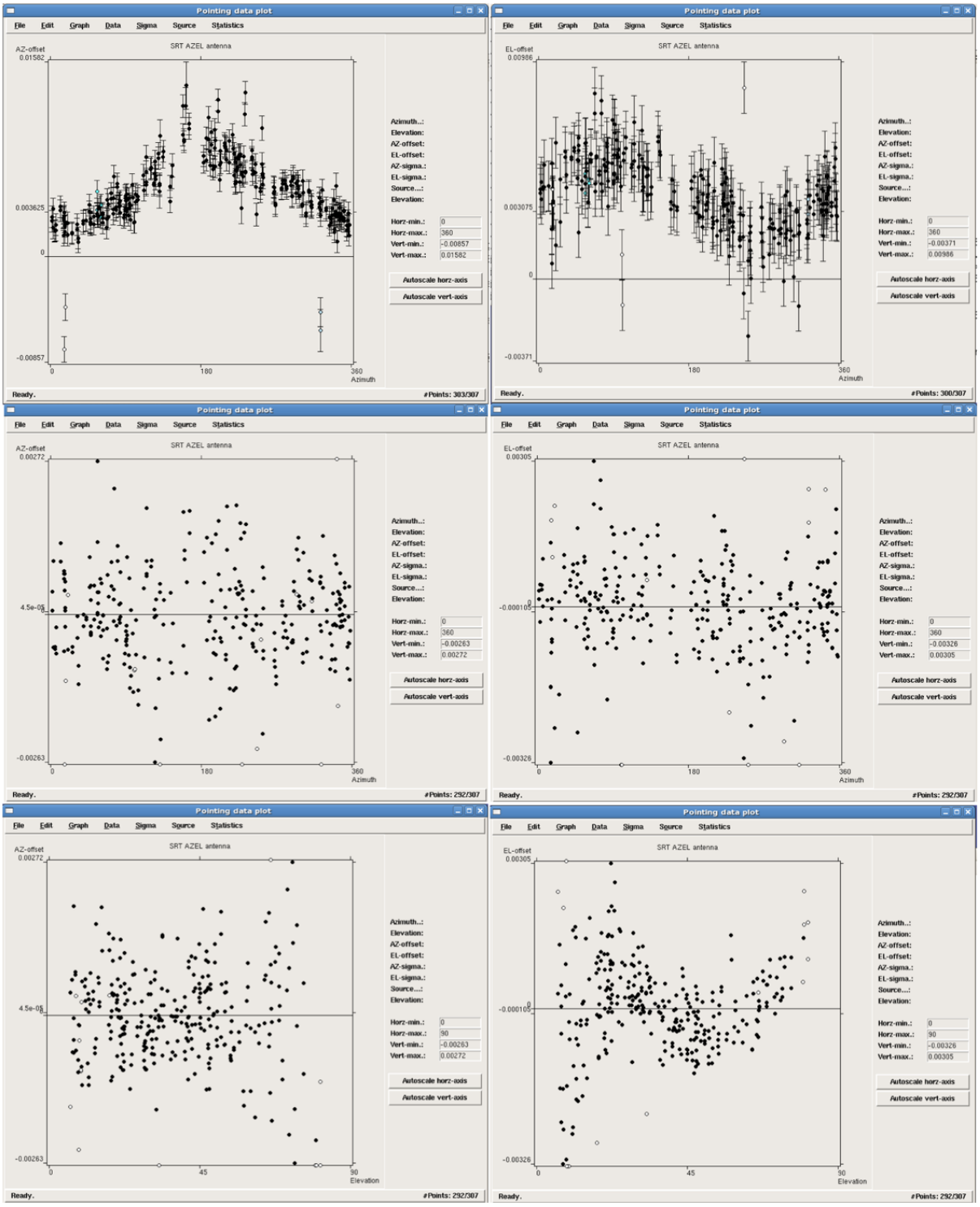

Figure B.2: *Raw data (top) and residuals (middle and bottom) after fitting the model. Flagged data are indicated with a white circle. The parameters of the new pointing model are saved in mdlpo_C_2017335.ctl (00005 2017 335).*

B) Check session of the C-band pointing model (mdlpo_C_2017335.ctl) using the observations carried out on 08/01/2018.

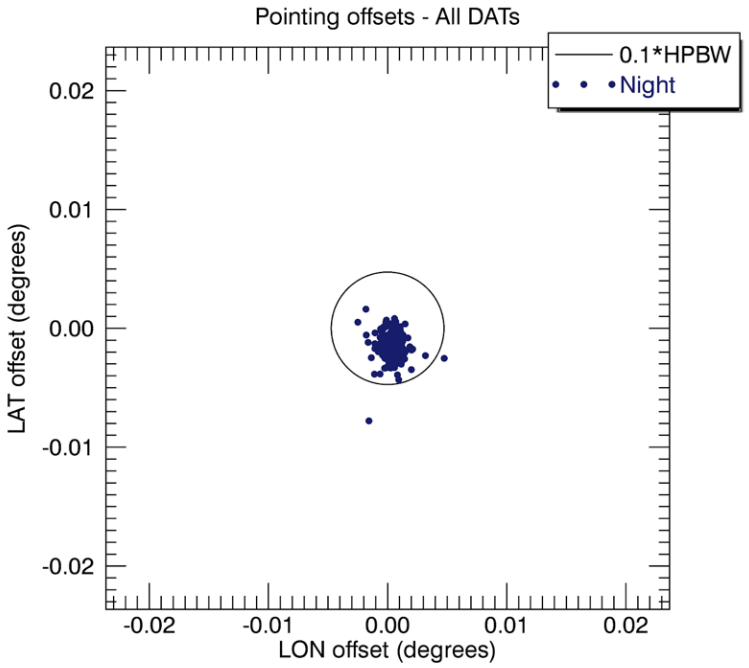

Figure B.3: *Raw offsets measured by applying the mdlpo_C_2017335.ctl model to the data acquired on 08/01/2018. Most of the offsets are lower than 1/10 of the HPBW (where HPBW=0.0473°), with an estimation of the distribution centroid at -0.002° in elevation and +0.001° in azimuth.*

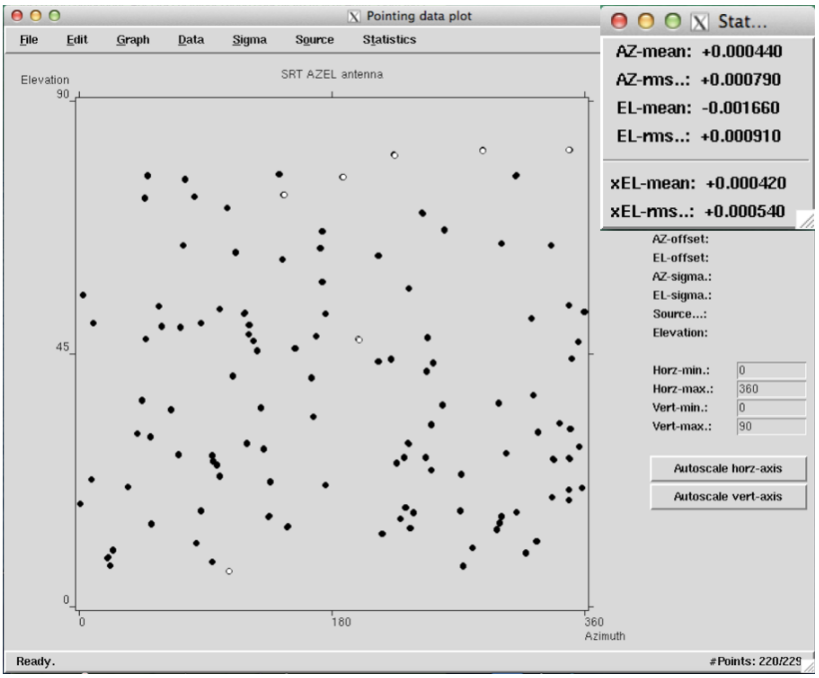

Figure B.4*: Az-El coverage of the 08/01/2018 dataset consisting of 229 points.*

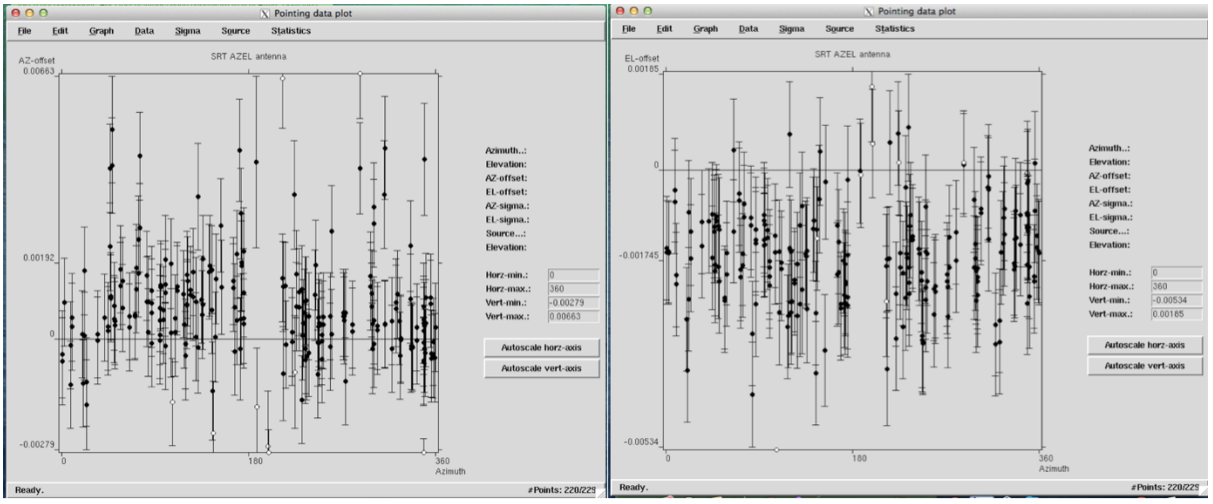

***Figure B.5**: Az-offset vs Azimuth (left) and El-offset vs Azimuth (right).*

C) Creation of a new pointing model on 22/12/2020 (mdlpo_C_2020069.ctl) based on the observations performed on 02/09/2020.

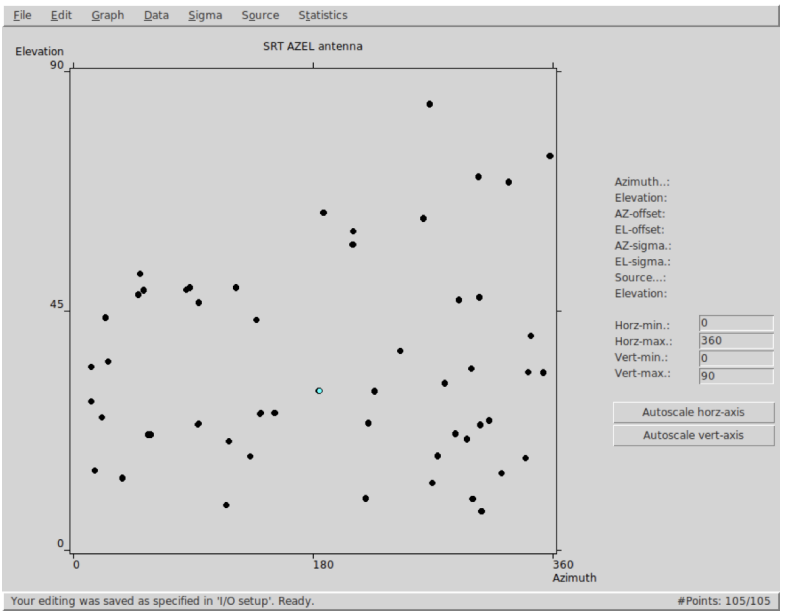

***Figure B.6**: Az-El coverage of the datasets obtained on 02/09/2020 consisting of 105 points (session of only 2 hours).*

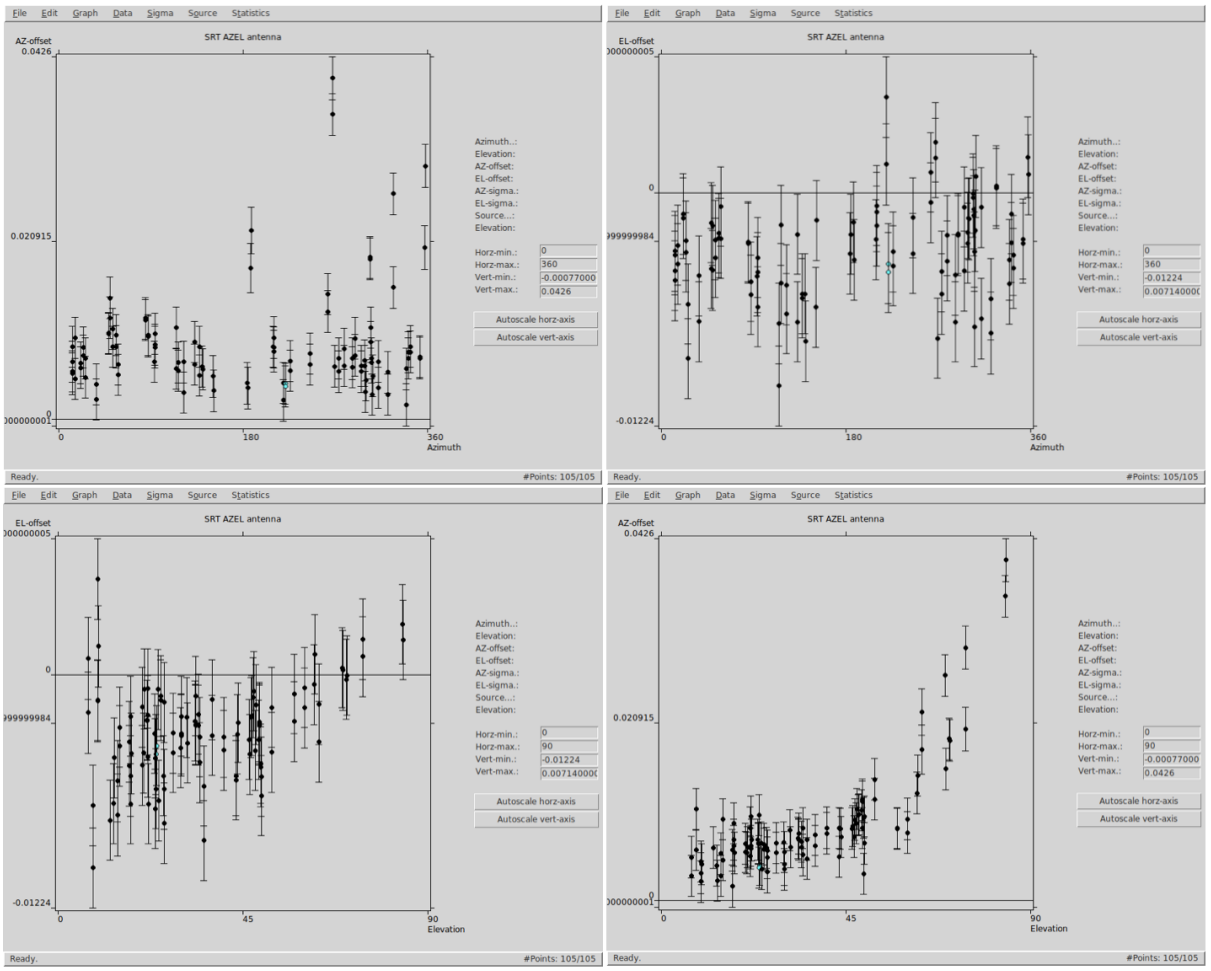

Figure B.7: *Raw data showing the different Az- and El-offset vs azimuth and elevation obtained on 02/09/2020.*

D) Refinement of the pointing model mdlpo_C_2020069.ctl on 15/12/2021 based on the observations performed on 12/02/2021. The new pointing model corresponds to mdlpo_C_2021349.ctl.

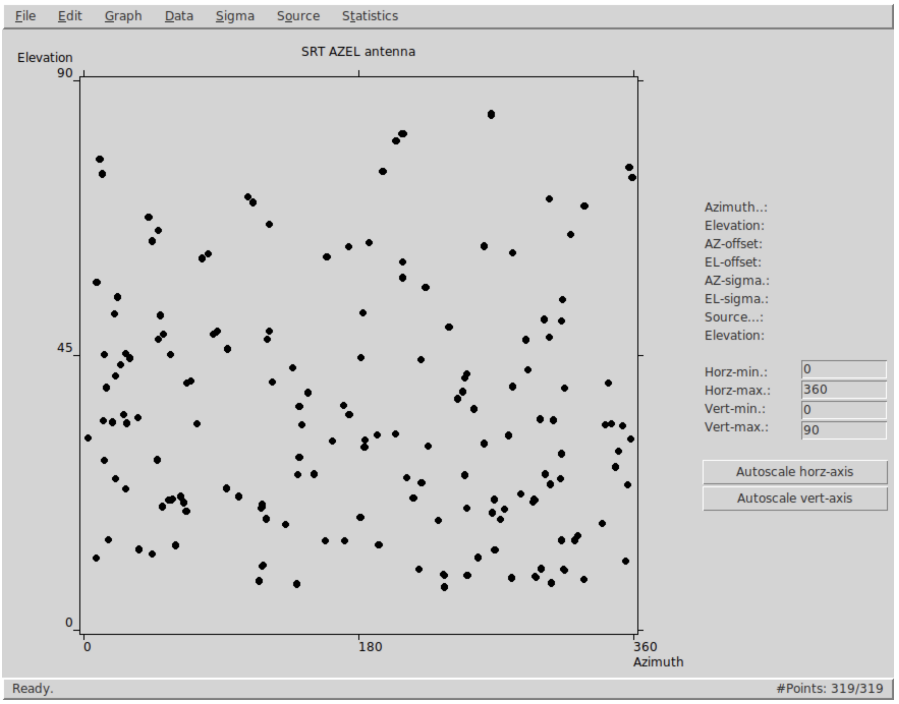

***Figure B.8**: Az-El coverage of the datasets obtained on 12/02/2021 consisting of 329 points (session of 6 hours).*

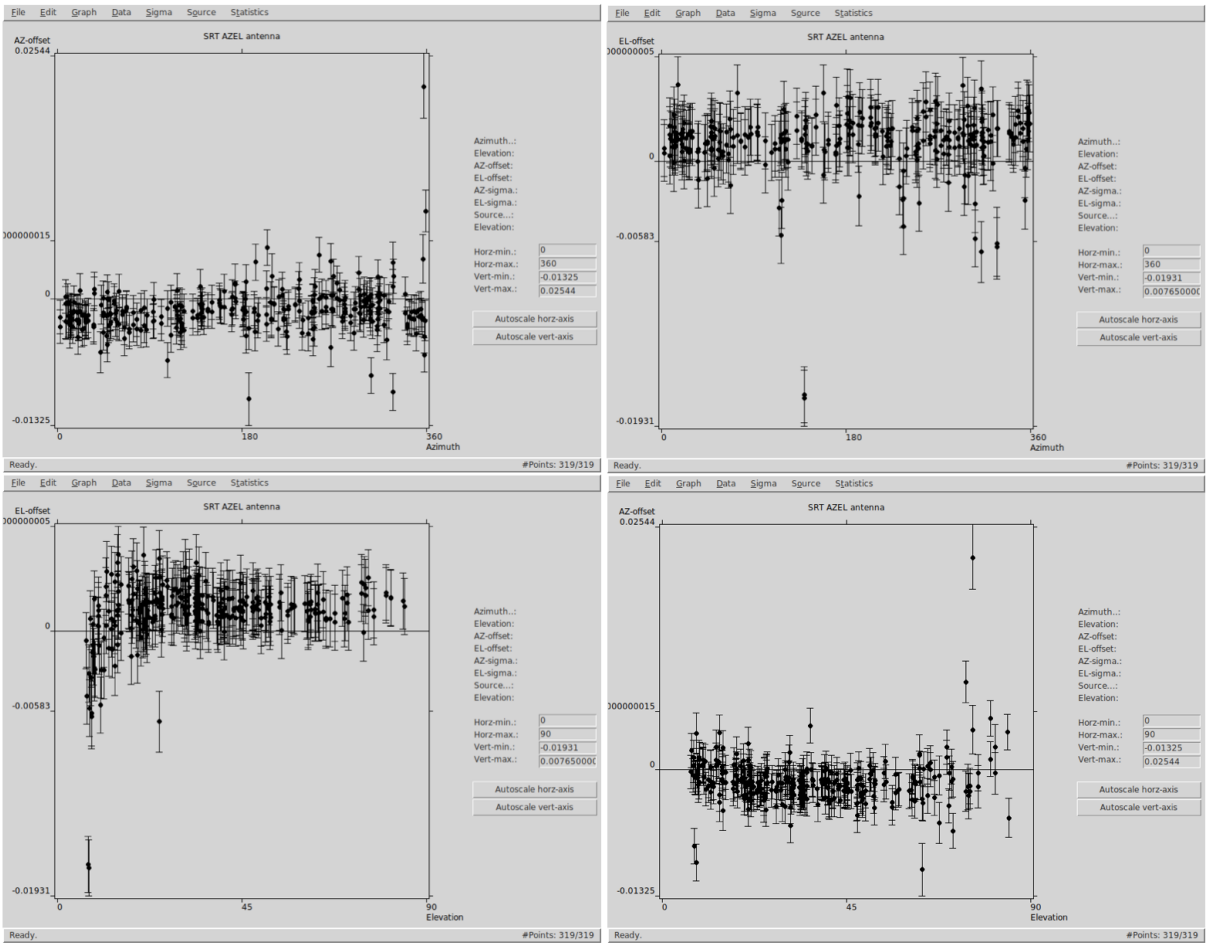

***Figure B.9:** Raw data obtained on 12/02/2021 showing the different Az and El-offset vs azimuth and elevation.*

2) Pointing model in K-band

A) Creation of a new pointing model in 2018 during the recommissioning (err2018.136) based on different observations performed in K-band. The 5th observation was carried out on 16/05/2018.

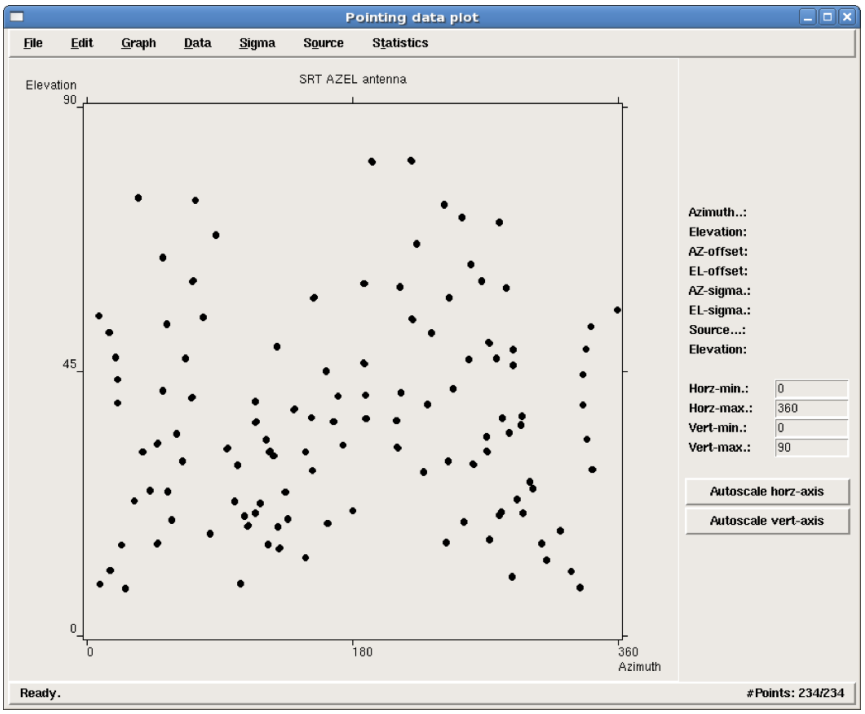

***Figure B.10**: Az-El coverage of the datasets consisting of 234 points (each point represents an Az/El cross-scan).*

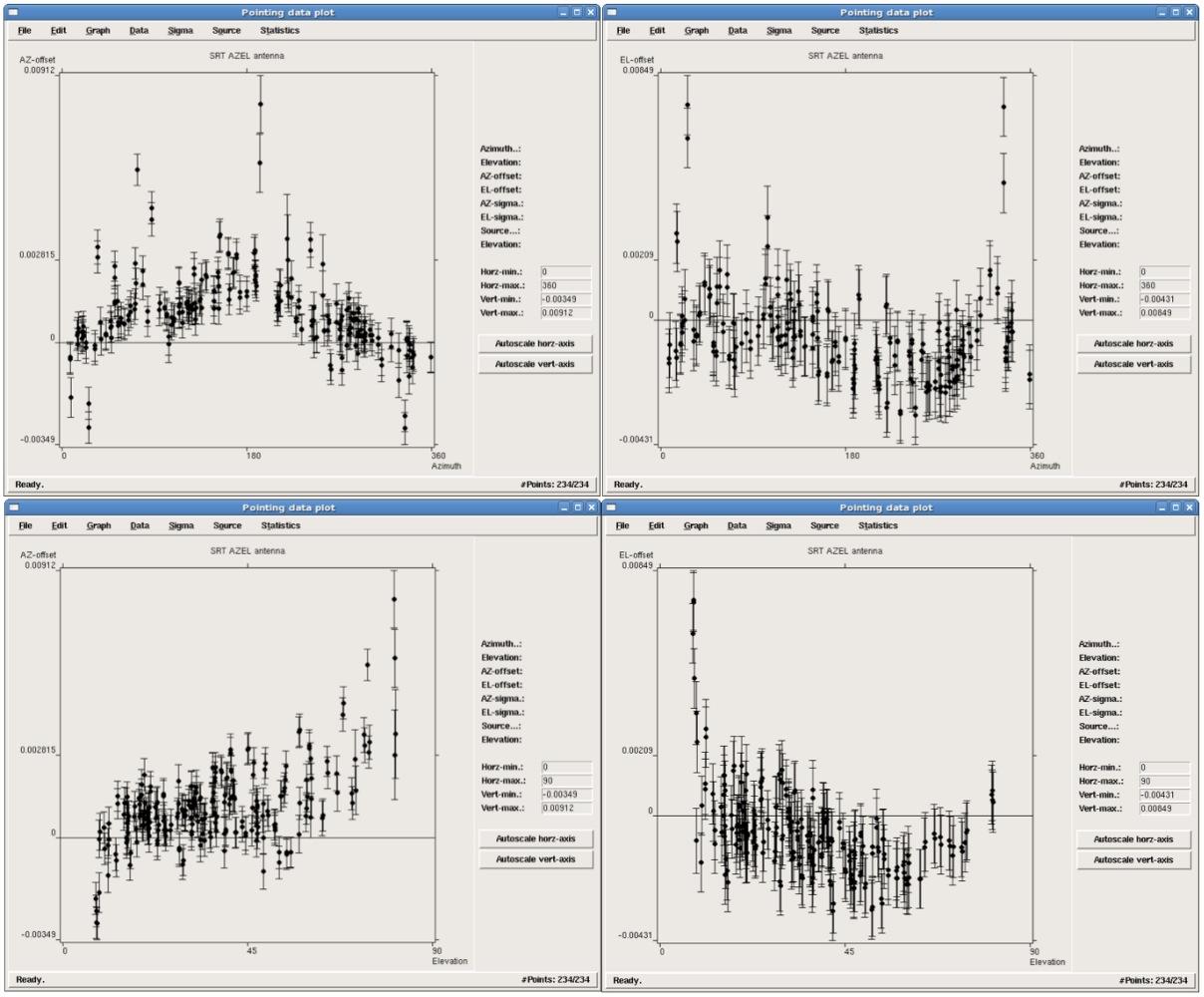

Figure B.11: *Raw data obtained on 16/05/2018 showing the different Az and El-offset vs azimuth and elevation.*

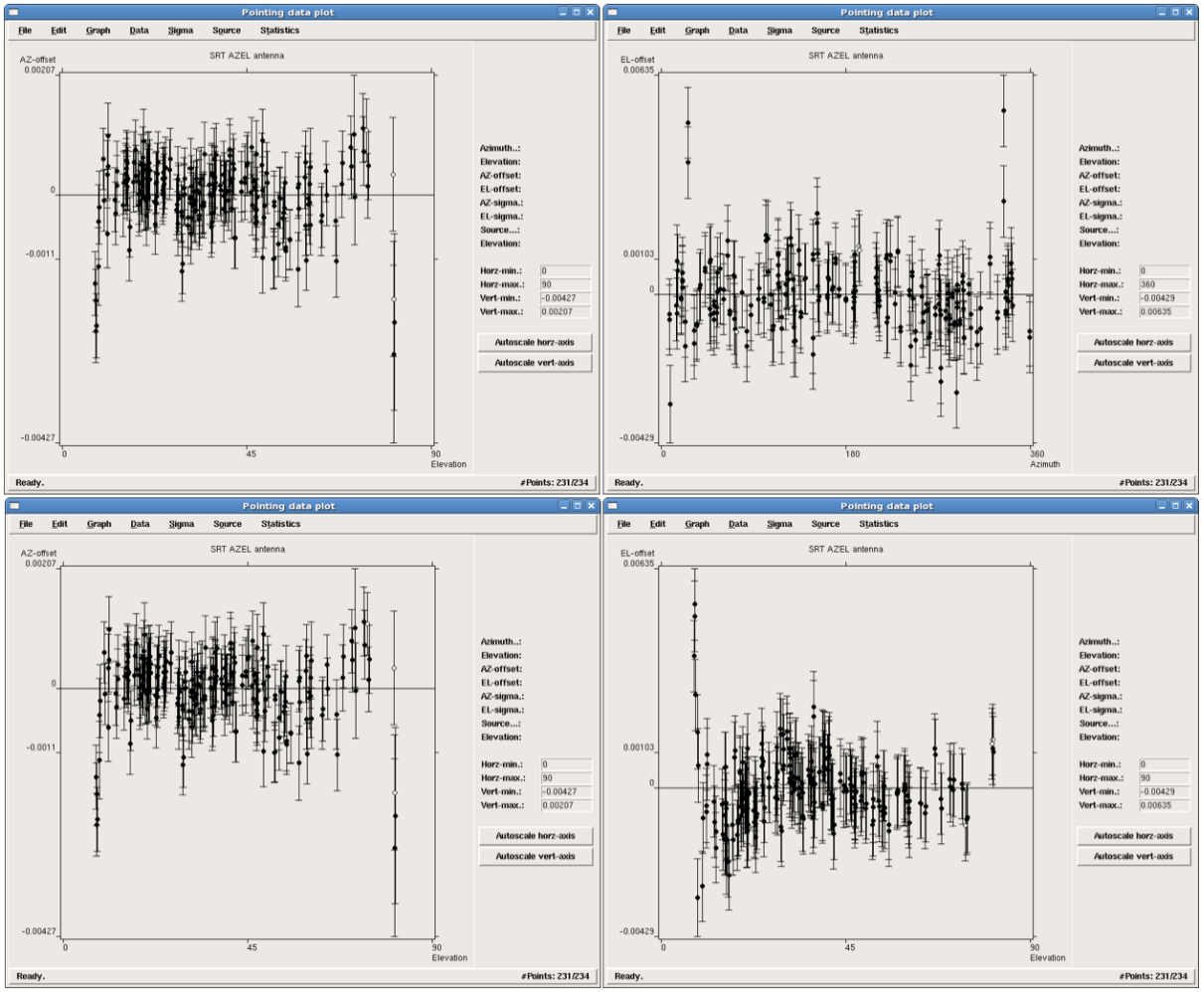

Figure B.12: *Data obtained on 16/05/2018 fitted by the model (flagging of 3 points).*

B) Creation of a new pointing model on 15/12/2021 based on the observations performed on 18/09/2020.

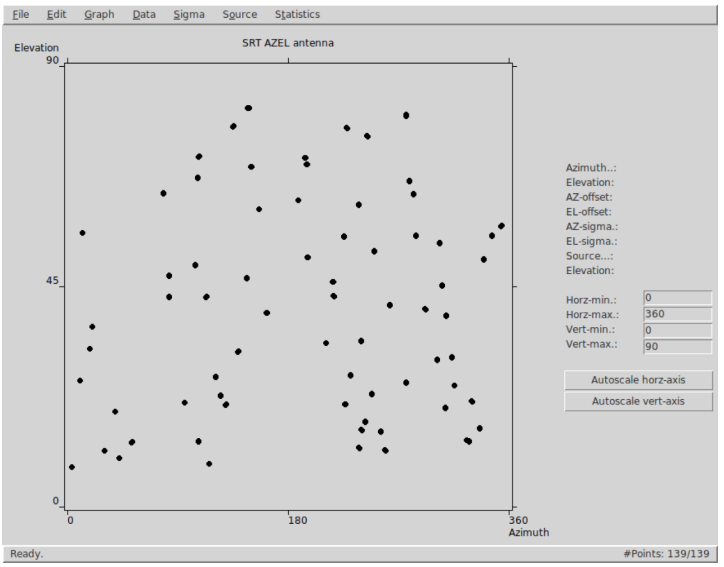

Figure B.13*: Az-El coverage of the datasets consisting of 139 points (each point represents an Az/El cross-scan).*

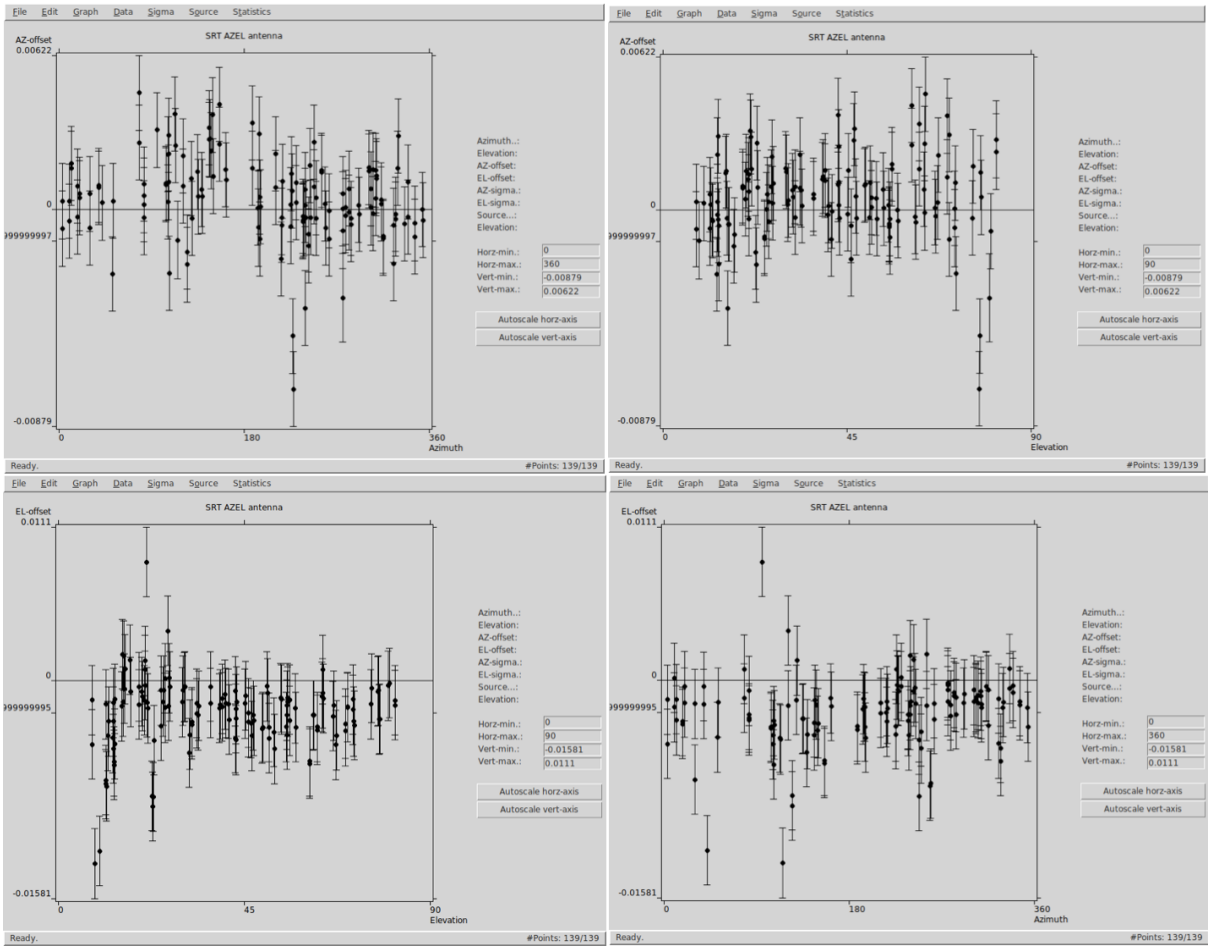

Figure B.14: *Raw data obtained on 18/09/2020 showing the different Az and El-offset vs azimuth and elevation.*

References

- Attoli et al. 2022a, Structures, https://doi.org/10.1016/j.istruc.2022.03.065
- Attoli et al. 2022b, SPIE Astronomical Telescopes + Instrumentation 2022, (submitted)
- Britzen et al. 2019, Galaxies, vol. 7, issue 3, p. 72
- Buffa et al. 2020, Proceedings Society of Photo-Optical Instrumentation Engineers (SPIE), 11445, https://doi.org/10.1117/12.2561787
- Bolli et al. 2015, Journal Astronomical Instrumentation., 4, 1550008
- D'Alessandro et al. 2022, EPJ Web Conf., 257 (2022) 00012, doi 10.1051/epjconf/202225700012
- Egron et al. 2017, Monthly Notices of the Royal Astronomical Society, 470, 2, p.1329-1341
- Govoni et al. 2021, XXXIVth General Assembly and Scientific Symposium of the International Union of Radio Science (URSI GASS),pp.1-4, doi: 10.23919/URSIGASS51995.2021.9560570
- Loru et al. 2019, Monthly Notices of the Royal Astronomical Society, 482, 3, p.3857-3867
- Melis et al. 2018, Journal of Astronomical Instrumentation, 7, 1, id. 1850004
- Murgia et al. 2016, Monthly Notices of the Royal Astronomical Society, 461, 4, p.3516-3532
- Navarrini et al. 2022, IEEE Access, doi: 10.1109/ACCESS.2022.3153492
- Orfei et al. 2010, IEEE Antennas and Propagation Magazine, vol. 52, issue 4, pp. 62-72
- Orfei et al. 2011, "Caratterizzazione del ricevitore nella banda 5.7-7.7 GHz", INAF SRT Memo Ser., Bologna, Italy, Tech. Rep. GAI04 FR 5.0, May 2011
- Orlati et al. 2016, Internal Report IRA 500-16 https://www.ira.inaf.it/Library/rapp-int/500-16.pdf
- Perrodin et al. 2016, 14th Marcel Grossmann meeting, arXiv:1608.01839
- Prandoni et al. 2017, Astronomy & Astrophysics, 608, A40, 26 pp.
- Recommissioning report 2019: SUMMARY https://docs.google.com/document/d/1OPdS_HAibSZ2BwwSd900wonI0lUcltI7l_F0MG4Auh0/
- Ricci et al. 2016, Internal Report INAF IRA 496/16
- Süss et al. 2012, Proceedings Society of Photo-Optical Instrumentation Engineers (SPIE), 8444, https://doi.org/10.1117/12.926141
- Tarchi et al. 2013, Internal Report INAF-OAC N.27
- G. Valente et al., "The Coaxial L-P Cryogenic Receiver of the Sardinia Radio Telescope," in IEEE Access, vol. 10, pp. 2631-2645, 2022, doi: 10.1109/ACCESS.2021.3139744.
- G. Valente, M.N. Iacolina et al., "The Sardinia Space Communication Asset: Performance of the Sardinia Deep Space Antenna X-Band Downlink Capability," in IEEE Access, vol. 10, pp. 64525-64534, 2022, doi: 10.1109/ACCESS.2022.3183745.

Acknowledgments

The Sardinia Radio Telescope is funded by the Department of University and Research (MIUR), the Italian Space Agency (ASI), and the Autonomous Region of Sardinia (RAS), and is operated as a National Facility by the National Institute for Astrophysics (INAF). The Enhancement of the Sardinia Radio Telescope (SRT) for the study of the Universe at high radio frequencies is financially supported by the National Operative Program (Programma Operativo Nazionale - PON) of the Italian Ministry of University and Research "Research and Innovation 2014-2020", Notice D.D. 424 of 28/02/2018 for the granting of funding aimed at strengthening research infrastructures, in implementation of the Action II.1 - Project Proposals PIR01_00010 and CIR01_00010.